Appendix E

Rock mass behaviour

E1 Closure measurements

E1.1 Introduction

Closure was measured at all three of the instrumentation sites to determine the rock mass behaviour in the stope and to provide information on pillar deformation. The measurements were compared to elastic models.

E1.2 Amandelbult 1-Shaft

The stope sheet in Figure E 1 shows the positions of the closure meters installed around Pillar 2 (P2). Both the up-dip stations were installed ahead of the down-dip face (Panel 13-16-2E). Both the up-dip and down-dip stations were installed about 2 m from the pillar edge and Gauge 3 was located at the centre of the ASG, about 1 m from the pillar. This closure meter was anchored approximately 0.5 m above and below the hangingwall and footwall of the ASG respectively. The measured closure was compared to an elastic model with a Young's Modulus of 80 GPa and a Poisson's Ratio of 0.23 in Figure E 2. These elastic constants were representative of the leuconorites and spotted anorthosites, the predominant rock type, and the lowest modulus of the geological sequence. The failed pillars were assumed to have a residual strength of about 20 MPa, which was approximately the measured strength at the site.

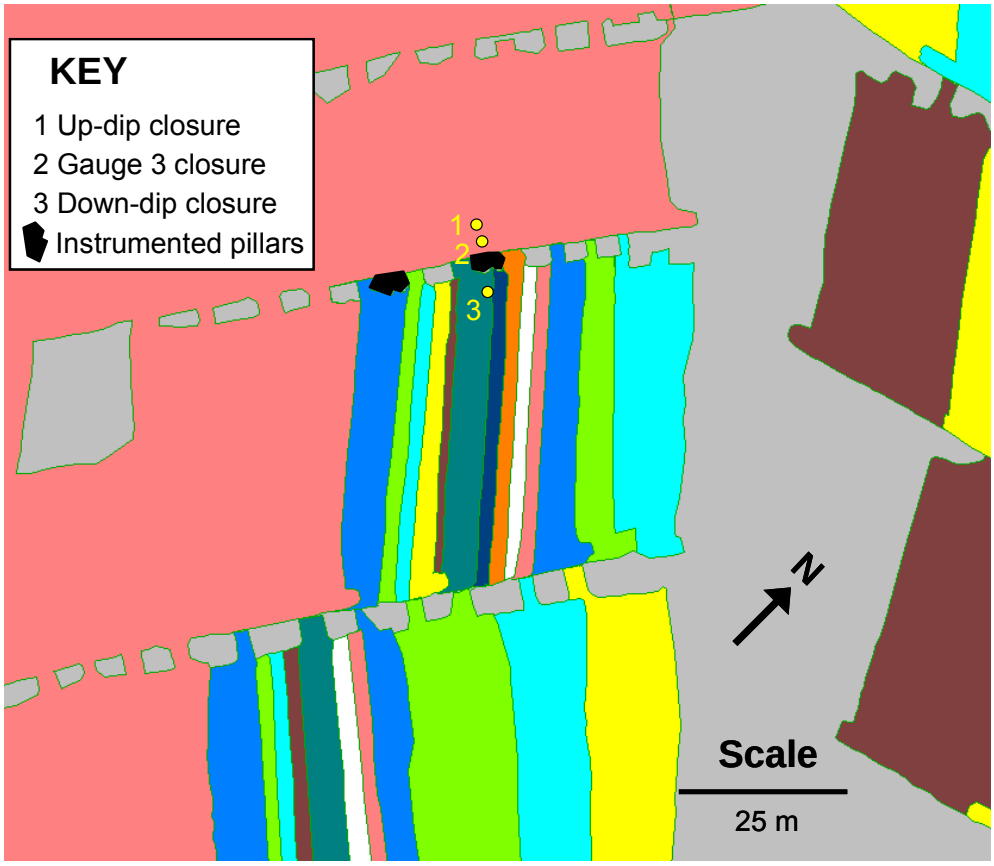

Figure E 1 Stope sheet showing the positions of the closure meters around P2

The closure meter on the down-dip side of the P2 was installed about 4 m behind the face and the measurements were similar to the elastic model (Figure E 2). However, on the up-dip side the measurements were significantly larger than the elastic model, particularly during the initial stages of pillar formation. The model assumed that the pillar failed when the face had advanced by about 3 m from the pillar edge, and that the residual strength dropped immediately after failure to 20 MPa. In reality, the pillar failed as it was exposed and the stress dropped to residual strength at a face advance of about 16 m. At least some of the additional measured closure occurred as a result of the mismatch between the model and reality. However, closure measurements made at face advances beyond 16 m still showed higher closure than what was modelled, suggesting an inelastic component of closure on the up-dip side of the pillar. A few open discontinuities were observed in the hangingwall up to a height of 4.25 m above the stope (in a

vertical borehole drilled at the centre of the stope), but these discontinuities could not account for the additional closure that was measured.

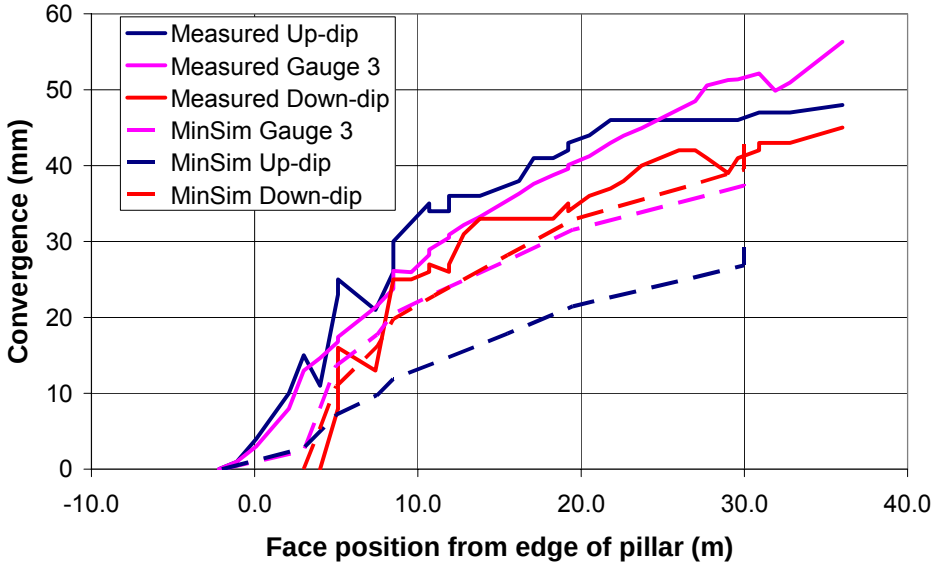

Figure E 2 Measured closure and elastic convergence at the Amandelbult site

1.8 m long jumpers were cemented into the centre of both the instrumeted pillars, near the top edge of the pillars and about 1 m vertically below this position as shown in Figure E 3A. A slow but perpetual upwards rotation was observed on the lower bar on both pillars as shown in Figure E 3B. This rotation could have resulted from sliding wedges in the pillar, but is more likely to be caused by a relatively larger downwards deformation of the more solid pillar centres than near the edge of the pillars. Also in both instances very little or no rotation occurred on the top bar and the direction of rotation on the lower bar was the same. The rotation of the bars and the additional measured closure suggest that the pillars were punching into the footwall with a flow of damaged footwall rocks into the gully on the up-dip side of the pillars. The measurements on Gauge 3 suggest that some of the inelastic deformation was occurring deeper than 0.5 m below the level of the ASG.

Figure E 3 Rotation of jumpers cemented into the centre of P2 near the top edge of the pillar and about 1 m vertically below. A = pillar failure, B = three months after pillar failure

E1.3 Impala 10-Shaft

The locations of the closure and closure-ride meter stations are shown in Figure E 4. The stations in Panel 7s were spaced approximately 2 m apart on dip. Panel 7s reached the face position denoted by the light blue in Figure E 4 before mining commenced in Panel 8s (up-dip) and very little mining had been done in Panel 6s (down-dip). Thus closure was measured in an isolated panel (without the influence of pillars) and is compared to an elastic model in Figure E 5 to determine the component of inelastic closure. The elastic model assumed a modulus of 15 GPa which was the secant modulus of the predominant rock type (Spotted Anorthosite) at a stress level of 30 MPa. This modulus provides the maximum possible elastic deformations and assumes that all the rock influencing closure is microfractured and nonlinear (Chapter 3). The inelastic components of closure were determined by subtracting the elastic convergence (assuming E=15 GPa and v = 0.32) from the measurements and the results are shown in Figure E 6. A reasonable correlation between the measured and elastic results

was obtained around the centre of the panel when the face advanced from 6.5 m to 11.8 m from the line of closure meters. The comparatively higher than elastic closure at the edge of the panel and the additional closure at further face advances is suggestive of buckling (York et al, 1998) or abutment punching. Extensometers and borehole camera surveys indicate that almost all of the fracturing occurred in the footwall. The comparatively higher closure measured on the down-dip side of the panel may be the result of inelastic flow of the footwall into the advanced strike gully (ASG) at the bottom of the panel. (Significant ride was observed on the closure meter adjacent to this gully.)

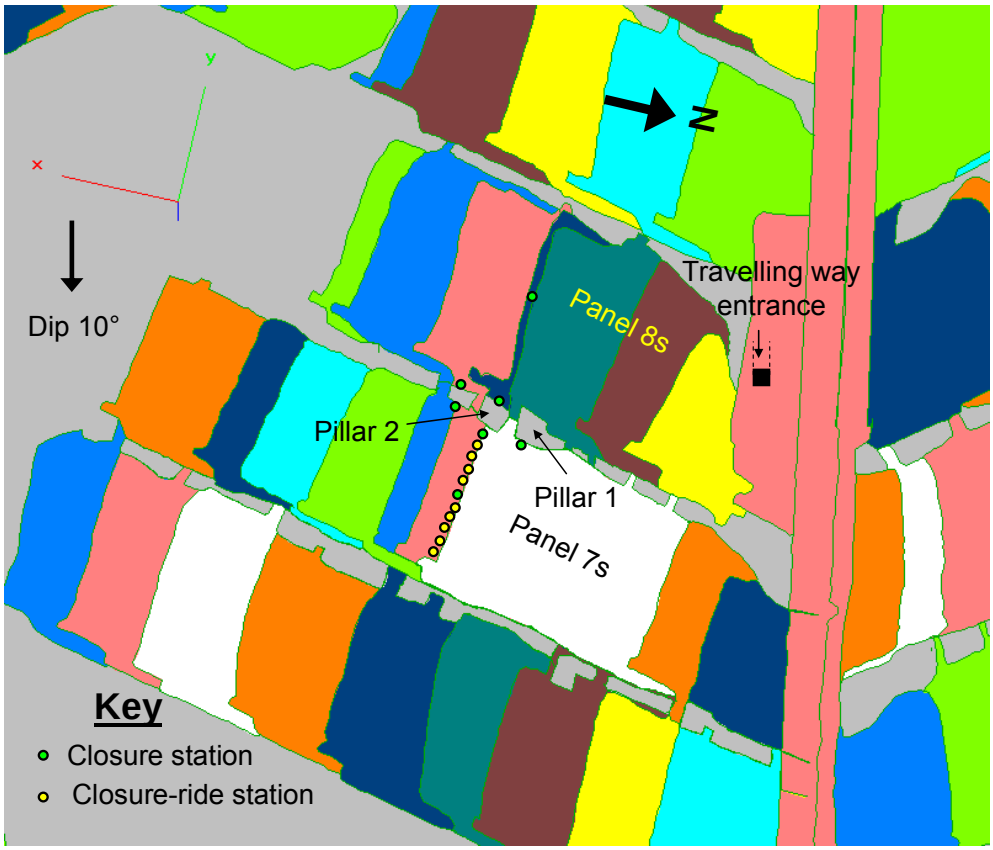

Figure E 4 Stope sheet showing the locations of the closure and closure-ride stations at Impala 10-Shaft

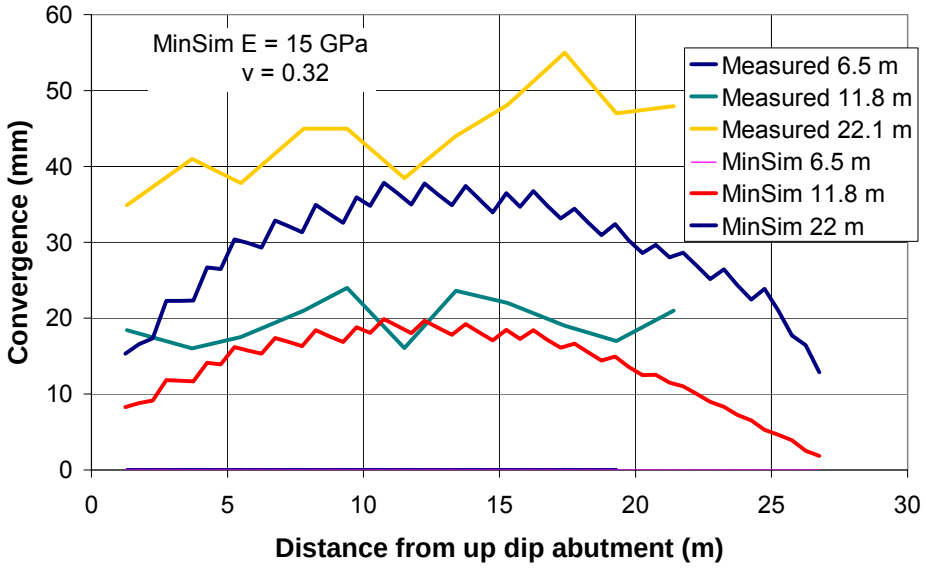

Figure E 5 Comparison between the measured closure and MinSim convergence for the isolated 7s panel at Impala 10-Shaft

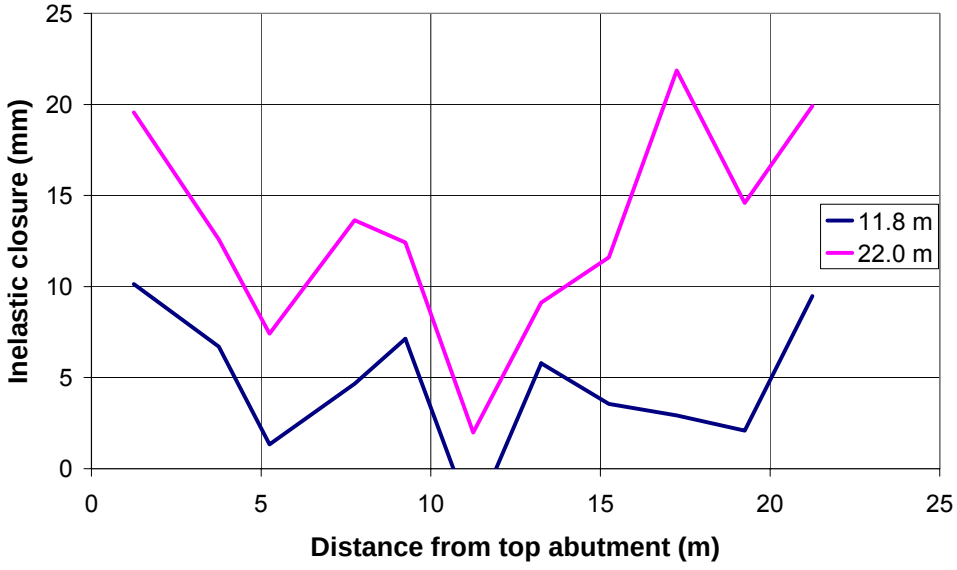

Figure E 6 Inelastic component of the measured closure for various face advances (assuming E=15 GPa)

The almost linear closure across the panel in Figure E 5 suggests bulking, possibly due to the fracturing of the footwall at the face. Figure E 7 shows that about 40 mm less closure actually occurred within 6 m of the face than predicted by the elastic model (with a Young's Modulus of 15 GPa and a Poisson's Ratio of 0.32). An explanation for the comparatively small deformation actually measured near the face is the affect on closure of the material above the face which is not microfractured. The model only accounts for a single modulus and therefore predicts more convergence near the face. As the closure was probably affected by linear elastic and microfractured rock above the panel, it is probable that some inelastic deformation is hidden in the low modulus used in the model. Thus some extension fracturing and bulking due to the drop in the vertical confining stress is possible, but is unlikely to be significant unless shear fractures developed ahead of the face, i.e. prior to the installation of the closure meter. These types of fractures were not observed in the hangingwall or footwall and the face also appeared unfractured when the panel was isolated. The closure that was measured at the centre of the panel from about 6 m face advance was almost elastic during the isolated stope conditions as shown by the dashed line in Figure E 7.

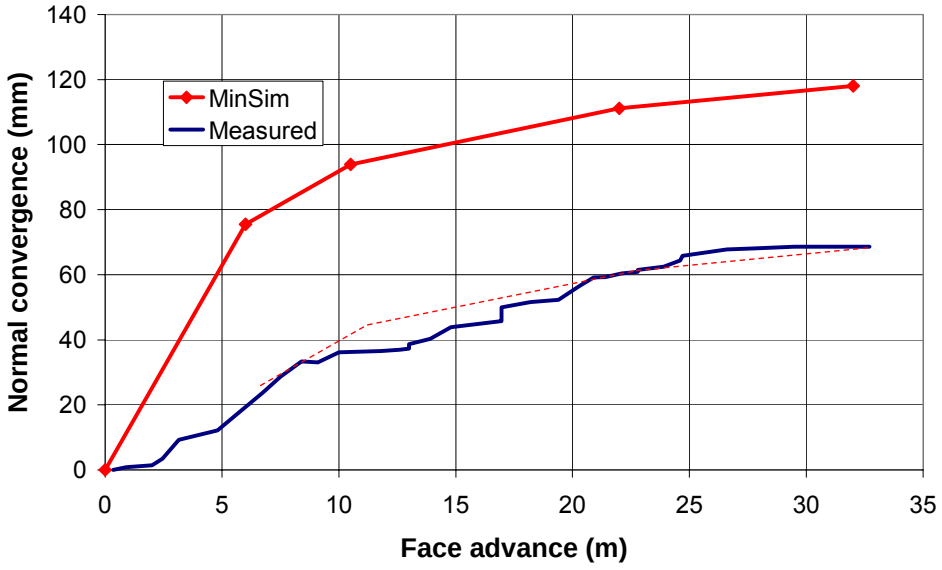

Figure E 7 Measured closure and elastic convergence at the centre of the panel

York et al (1998) shows that the heave near the abutments in Figure E 6 could be associated with buckling. In the scenario shown in Figure E 8, York et al (1998) suggests that the initial heave results from discontinuities or fractures closer than 1 m to the excavation. The secondary buckling at higher face advance may have occurred at deeper levels.

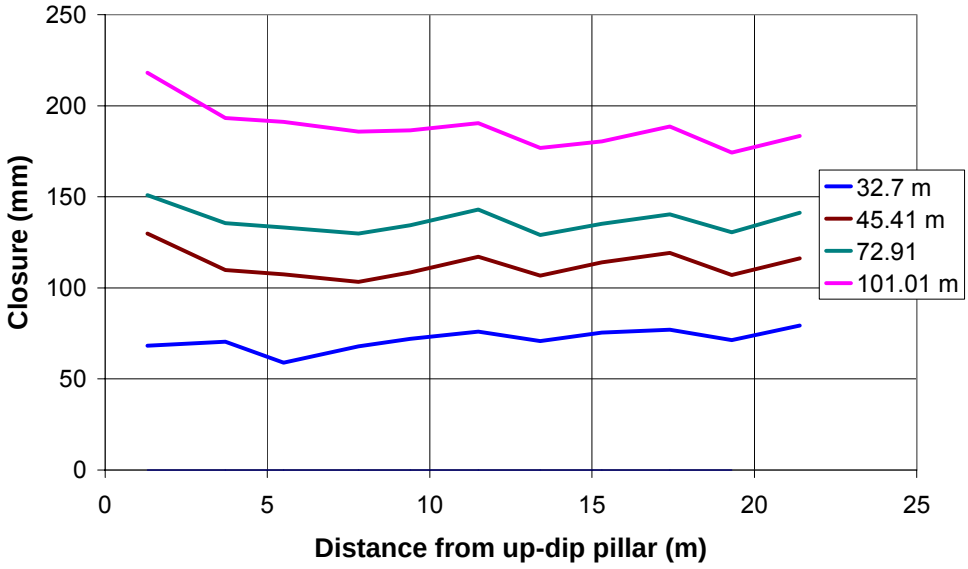

Figure E 8 Closure measured at various face advances of Panel 7s. Pillar formation occurred between face advances of 32.7 m and 101.01 m

The 15 GPa modulus used in the isolated panel models was not applicable when the pillars between panels started crushing. Such a low modulus in the models provided elastic closures that were significantly greater than the measurements. An explanation for the apparent reduction in the closure rate once the pillars were formed is that an increased span across several panels resulted in an increased height of rock influencing closure and thus a greater percentage of rock was not microfractured than in the isolated panel. As subsequent mining resulted in greater spans, the influence of the linear, higher modulus rock became greater and therefore the representative modulus also changed with each mining step. Failure of the pillars on the up-dip side of the panel, between face advances of 32.7 m and 45.41 m, resulted in relatively more closure adjacent to the abutment/pillar as expected (Figure E 8). Further heave appears to have

occurred after the pillars reached their residual state as shown by the increased slope of the curves on the up-dip side of the panel, between 72.91 m and 101.01 m in Figure E 8.

The closures represented in Figure E 8 were plotted against time in Figure E 9. The first 33 m face advance in Figure E 6 and Figure E 8 shows the closure in the isolated panel. Face advance was temporarily halted in Panel 7s between 9 December 2005 and 31 March 2006. During this time mining commenced in Panel 8s and the face in Panel 6s was also advanced as shown by the yellow in Figure E 4. This mining resulted in a comparatively lower closure rate than the isolated panel, due in part to the reduction in elastic convergence. The closure rate gradually increased as the up-dip and down-dip faces approached the closure meter stations and the pillars in the vicinity of the closure meter stations failed. At the end of March 2006, the face in Panel 8s was temporarily halted in line with the closure meters in Panel 7s. Failure was also initiated on the pillars in line with the closure meters, which resulted in comparatively more closure immediately down-dip of the pillar between Panels 7s and 8s as shown by the pink line in Figure E 9. Mining was subsequently resumed in Panel 7s, which was mined together with Panel 6s until 14 June 2006, where mining was again temporarily halted in Panel 7s and resumed in Panel 8s. Panel 8s reached its final position on 25 August 2006, which coincided with a significant drop in the closure rate in Figure E 9. Subsequent mining in Panel 7s had a relatively small impact on closure.

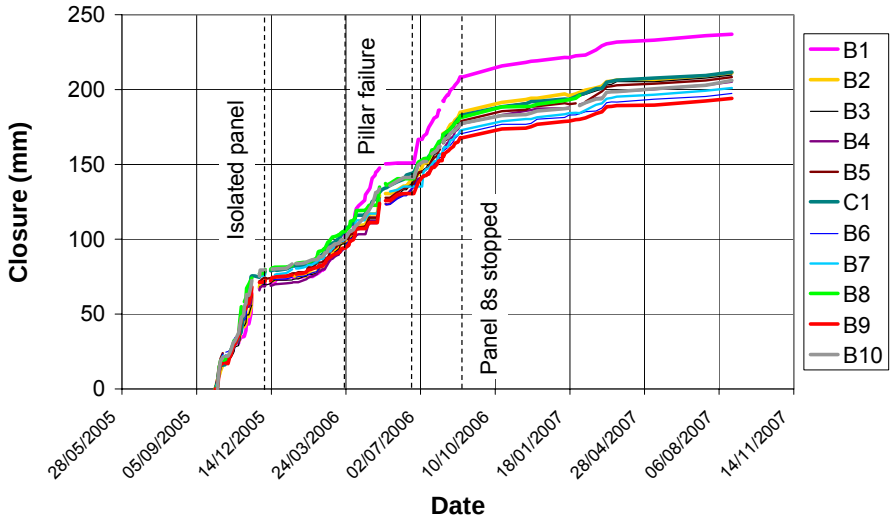

Figure E 9 Closure on the line of closuremeters shown in Figure E 4. B1 and B10 are at the top and bottom of the panel respectively

The high closure rate and comparatively greater closure on B1 than the other stations between April and July 2006 in Figure E 9, coincided with the formation and failure of the three instrumented pillars up-dip of the closure meter stations. The measured closure between June 2006 and August 2006 was mainly influenced by mining in Panel 8s as there was no mining in Panel 7s and the face was far advanced in Panel 6s during this period. The influence of the mining in Panel 8s on the closure in Panel 7s can clearly be seen in Figure E 9 when mining in this panel was stopped, even though mining resumed in Panel 7s. The strong influence of mining in Panel 8s on the closure in Panel 7s is suggestive of pillar failure and relatively low residual strength. An assessment of the pillar residual strengths is provided in Chapter 5.

Ride measurements were made at the centre of Panels 7s and 8s. The strike ride was small and noisy (Figure E 10). A movement of the footwall away from the face was confirmed by six of the seven stations located in Panels 7s and 8s (Figure E 4) and a discontinuity that intersected the travelling way about 1.3 m below the stope (Figure E 11). In the case of the discontinuity, approximately 60 mm of strike ride occurred in the rock above relative to the rock below this discontinuity. The travelling way was located near a large pillar (Figure E 4) that

failed seismically in the back area and the large strike ride on the discontinuity was probably influenced by this pillar. The elastic model shows very little strike ride (0.4 mm) but the general direction is also away from the face. The only station that did not show a net movement of the footwall away from the face was installed in an isolated panel. However, there was an initial displacement in this direction, which appears to have been overridden by other mechanisms that are not well understood. The opening of microfractures are suspected to have influenced the behaviour.

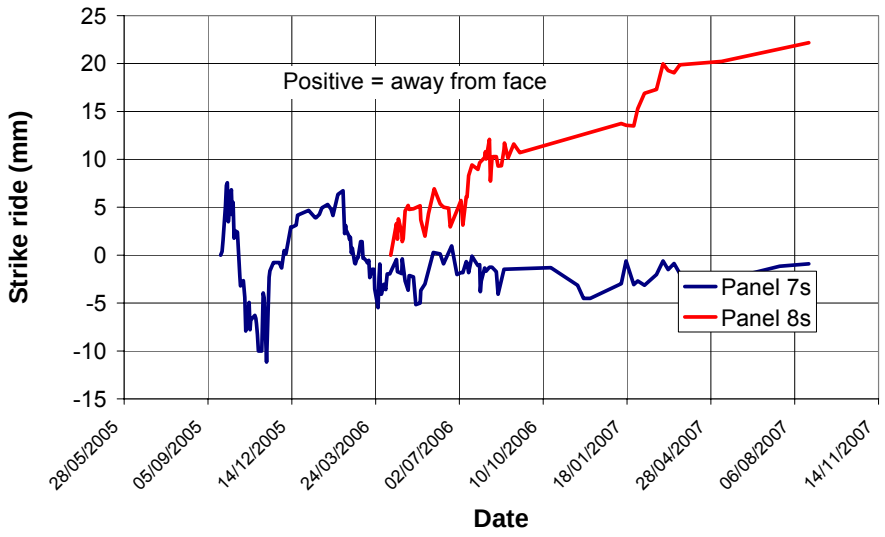

Figure E 10 Strike ride measurements at the centre of Panels 7s and 8s

Figure E 11 Movement on a structure in the footwall during the mining of Panel 8s

The dip ride measurements in Panel 7s showed an initial down-dip and a subsequent much stronger up-dip movement of the footwall relative to the hangingwall (Figure E 12). However, the footwall of the more highly stressed 8s panel only moved down-dip at the measurement point (which was installed about 0.5 m from the face). The elastic model shows an up-dip movement for both panels. The strong up-dip movements in Panel 7s are suspected to be the results of micro-cracking in the rock mass or from the development of the fractures that were later observed in the footwall (Section E3). The down-dip movement of the footwall in Panel 8s is suspected to have resulted from an overriding footwall punching affect of the large pillar at the top of panel 8s (Figure E 4). Once mining was initiated in panel 8s, an almost elastic ride response was observed in Panel 7s (Figure E 12). At this stage the face position in Panel 7s was far advanced and face advances were not made in the panel for several months. It appears that the original mechanism for the large-scale inelastic footwall ride in Panel 7s had been reduced or terminated.

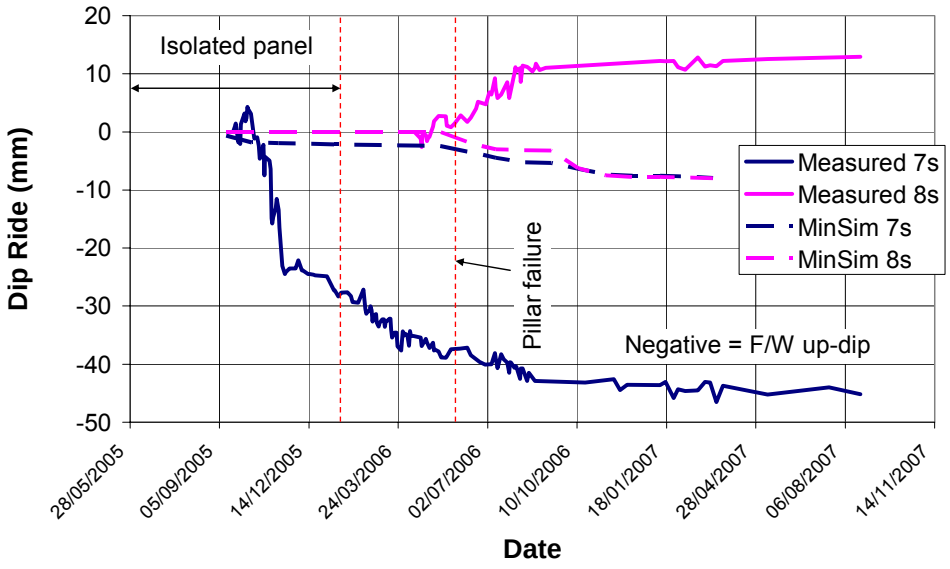

Figure E 12 Dip ride measurements at the centre of Panels 7s and 8s

Very small dip rides (5 mm to 10 mm) were measured adjacent to the monitored pillars at failure. Two of the pillars showed a comparatively larger movement of

the hangingwall away from the pillar and one indicated this movement to be in the footwall. The very small dip rides measured at the pillar and the net up-dip movement of the footwall at the centre of Panel 7s suggests that if footwall punching occurred, very little lateral deformations accompanied this punching.

E1.4 Union Spud shaft

Closure and closure-ride stations were installed on the north side of the monitored pillar (Figure E 13) in the 12 m ledging span, before the instrumented pillar had been cut. Measurements were made on a daily basis for a period of about 18 months and the results are shown in Figure E 14. The station to the north of the centre-raise (6.3 m in Figure E 14) was anchored 4.5 m below the centre-gully i.e. about 5.5 m below the normal footwall surface, to provide information on pillar strains. The mining sequence and pillar formation is shown in Chapter 2. The instrumented pillar failed when mining had advanced 5.2 m on either side of the pillar and a 2 m wide heading was excavated about 2 m behind the pillar from the down-dip side. The first closure meter to the south of the pillar was installed when the 2 m wide heading holed through to the up-dip workings and the pillar was formed. The APS had dropped to 80 MPa by this stage. Subsequent closure stations were installed when the APS of the instrumented pillar was below 50 MPa. An attempt to install a line of closure meters on dip was made but ground conditions were dangerous in the area and only three stations were installed. The 3S face was subsequently stopped prematurely.

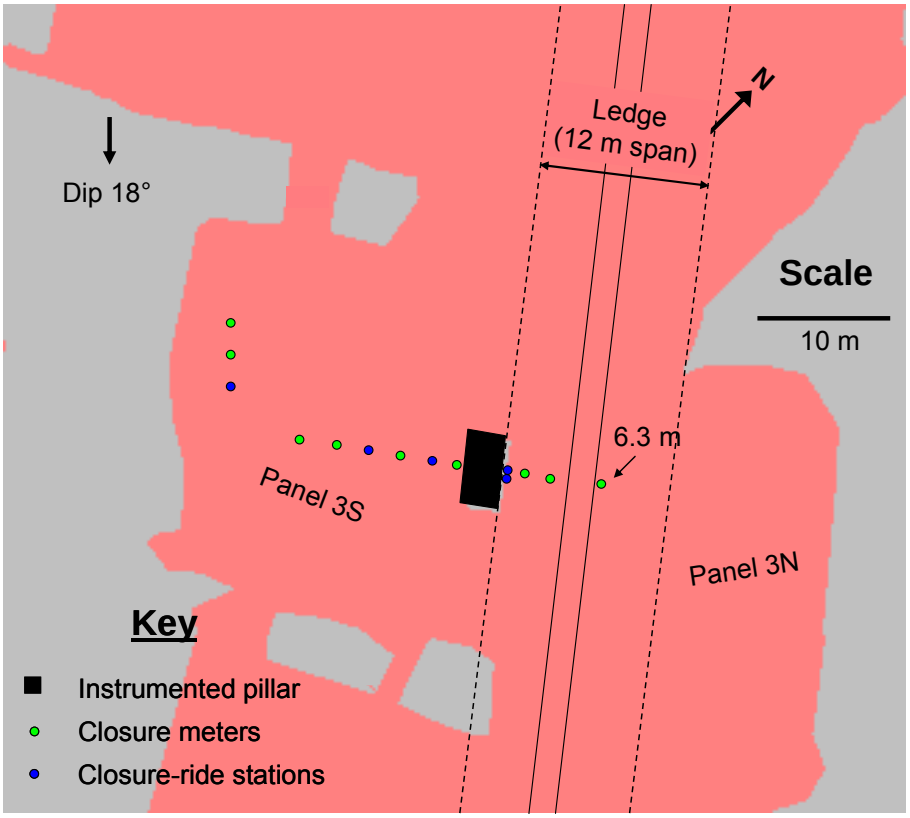

Figure E 13 Stope sheet showing the locations of the closure and closure-ride stations at the Union Spud shaft site

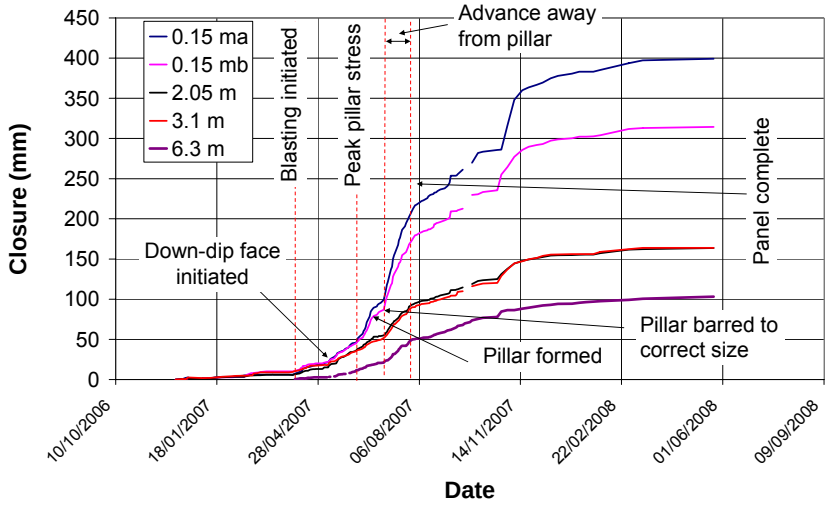

Figure E 14 Closure measurements made at various distances from the edge of the monitored pillar (towards the north)

The closure results in Figure E 14 show that a similar amount of closure (~8 mm) was measured by the four stations in the ledge adjacent to the proposed pillar for a period of four months prior to mining. The stations were located at 0.15 m, 2.05 m and 3.10 m from the proposed pillar edge. Since all the stations showed a similar change, the closure is suspected to be the product of deeper level foundation failure, bulking and possibly buckling with a small elastic component due to external mining. The core from an extensometer hole adjacent to the closure meter station on the north side of the centre raise (6.3 m) showed that the footwall was highly fractured to a depth of about 3 m below the stope (2 m in Figure E 15). This suggests that some inelastic closure had already occurred prior to the closure meter installations. The initial mining on the up-dip side of the pillar resulted in an increase in the closure rate particularly near the pillar, i.e. a profile of decreasing closure rate with distance from the pillar (Figure E 16). This profile could not be replicated with an elastic model (Figure E 17) (Young's modulus of 30 GPa and Poisson's Ratio of 0.32 were used in the model), and suggests inelastic behaviour due to pillar punching. The profiles in Figure E 17 suggest that a significant proportion of the inelastic deformations were occurring in the footwall at depths less than 5.5 m below the stope during this period (above the anchor in closure station 6.3 m). However, it is apparent from the initial measurements made on closure station 6.3 m that the modulus was too low, i.e. an exaggerated convergence is shown in Figure E 17.

Figure E 15 Core from the footwall extensometer

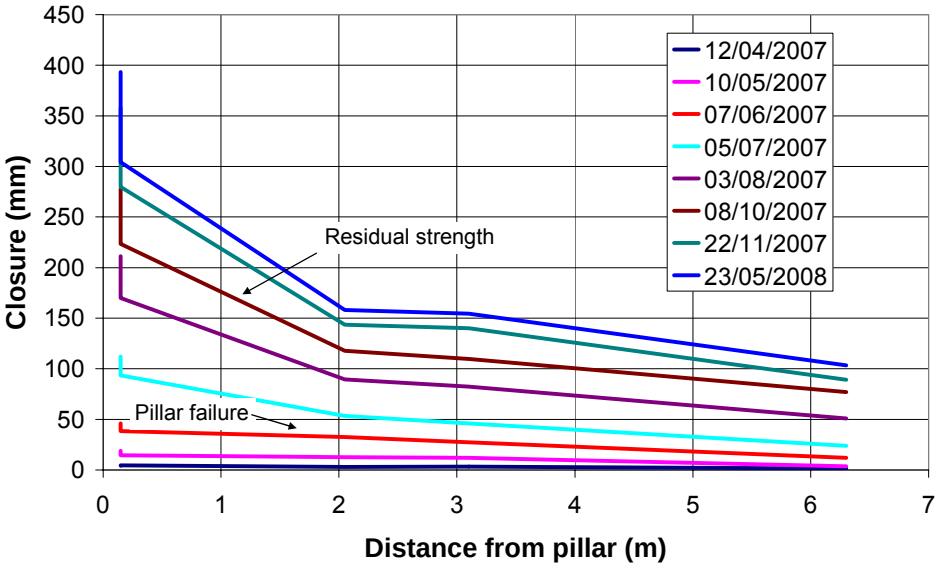

Figure E 16 Closure in the ledge with distance from the pillar edge

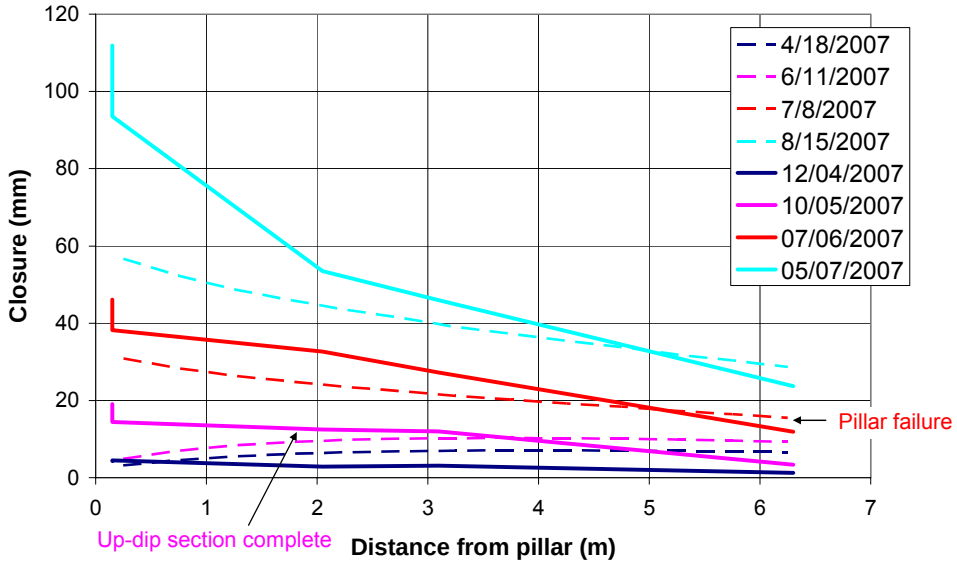

Figure E 17 Closure (solid lines) and elastic convergence (dashed lines) with distance from pillar edge

A significant increase in the closure rate occurred when mining was initiated on the down-dip side of the pillar (Figure E 14). At this stage significantly more

closure was measured adjacent to the pillar than at 2.05 m and 3.10 m. The additional closure was accompanied by footwall ride away from the pillar (Figure E 18), which also could not be replicated by an elastic model. The closure and ride measurements suggest pillar yielding and punching of the pillar stub into the footwall. The initial dip-ride was similar to the elastic model when a Modulus of 60 GPa and Poisson's Ratio of 0.32 was applied (Figure E 18). However, significant inelastic dip ride appears to have occurred when mining was initiated in the 3N panel. The abrupt increase in closure that occurred adjacent to the pillar at pillar failure is consistent with the relaxation of the strata during failure (Figure E 17). However, a different closure rate was observed on the two adjacent closure-ride stations during the mining of Panel 3S indicating inelastic closure, probably as a result of pillar punching. The different closure rates along the pillar edge were particularly noticeable during the mining of the 3N panel (Figure E 14). In addition, the comparatively higher closure rate measured adjacent to the pillar and the smaller but similar measurements at 2.05 m and 3.10 m could not be matched with an elastic model. A much smaller closure rate was measured on station 6.3 m than on the other closure meters during this time (Figure E 14), which is contrariwise to the elastic model as this station was closest to the mining face. These measurements suggest, therefore, that a significant amount of the inelastic deformations were occurring less than 5.5 m below the stope. Figure E 19 shows a large degree of inelastic closure adjacent to the pillar, which is suspected to be essentially shallow depth (Appendix C). However, the closure measured on stations 2.05 m and 3.10 m were similar to each other indicating the possibility of some deeper level inelastic processes. The closure on these stations could also have been influenced by mobilization of fractured material into the centre gully.

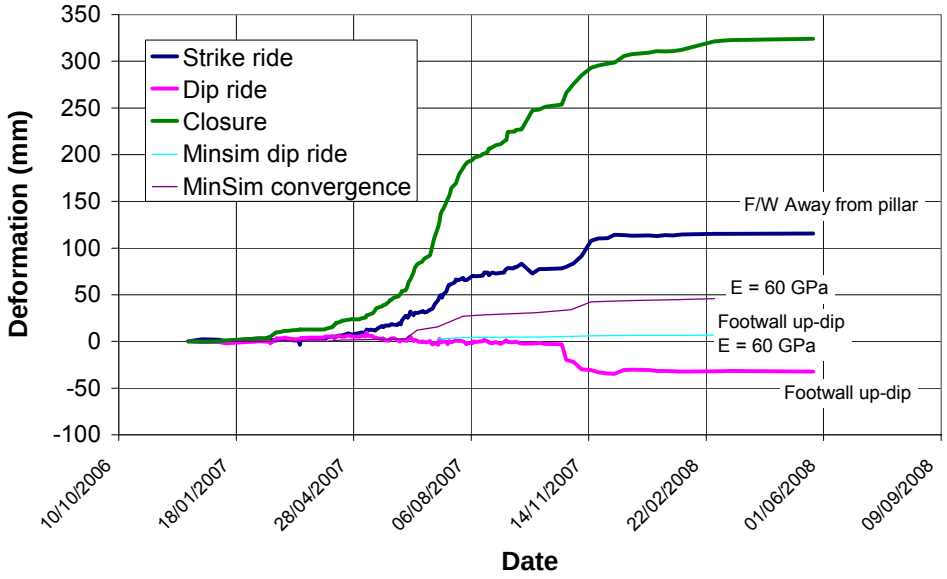

Figure E 18 Closure and ride measured at station 0.15 mb

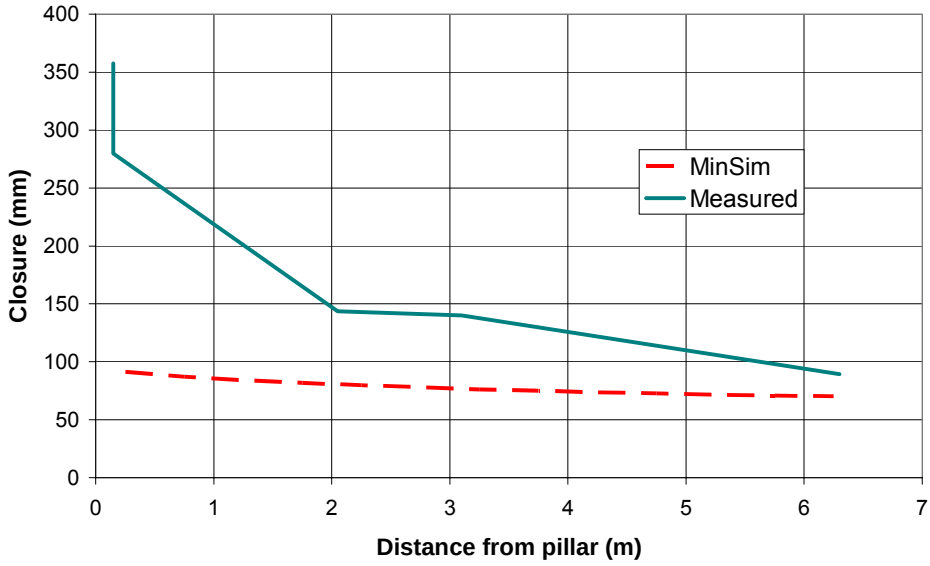

Figure E 19 Closure and elastic convergence at the edge of the monitored pillar from the start of mining in Panel 3S to completion of mining in Panel 3N

The closure measured on the line of stations along the centre of the panel in the strike direction (Figure E 13), are compared to an elastic model assuming a Young's Modulus of 15 GPa and Poisson's Ratio of 0.32 in Figure E 20 (crush pillars were given a residual strength of 15 MPa in the model). There is little correlation between the measured and modelled profiles. The closure varied considerably along the line of stations, which could be a partial explanation for the apparent random failure of the mine pole supports. The variation in closure along the panel was as well as the very low modulus in the elastic model indicates a high degree of inelastic behaviour that appears to mask the elastic component.

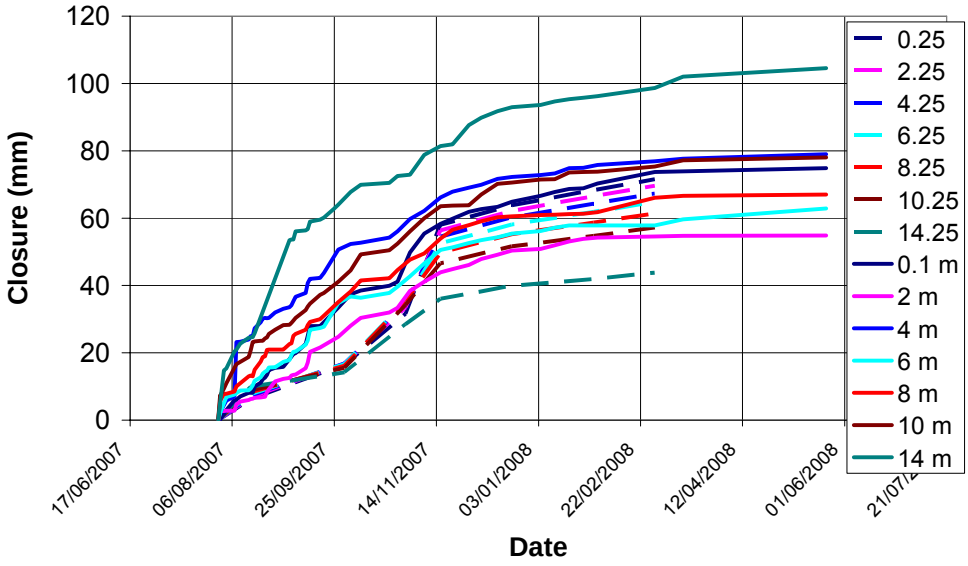

Figure E 20 Closure (solid lines) and elastic convergence (dashed lines) on the south side of the instrumented pillar

Figure E 21 shows the strike ride measurements at 2 m, 6 m and 14 m from the pillar edge. The station at 14 m was 6 m from the final position of the face and measurements were initiated when this station was 4 m from the face. During the mining of the 3S and 2S panels, the footwall moved away from the 3S face. However, after this mining was terminated there was a reversal in the direction of movement in the two stations closest to the pillar (Stations 2 m and 6 m). The shape of the closure profiles in Figure E 22 suggest that the pillar and probably the face were punching into the foundation rocks, and this is likely to be the

reason for the ride. It appears that the effects of the crushed pillar were overridden by the face during the initial mining but subsequent mining of the 3N and down-dip panels caused sufficient pillar punching to reverse the direction of the ride on stations 2 m and 6 m. The residual pillar stress was reached before 26/10/2007 but the ride continued on the station at 2 m. Further steepening at the pillar edge of subsequent closure curves in Figure E 22 is evidence of the pillar influence on stope behaviour.

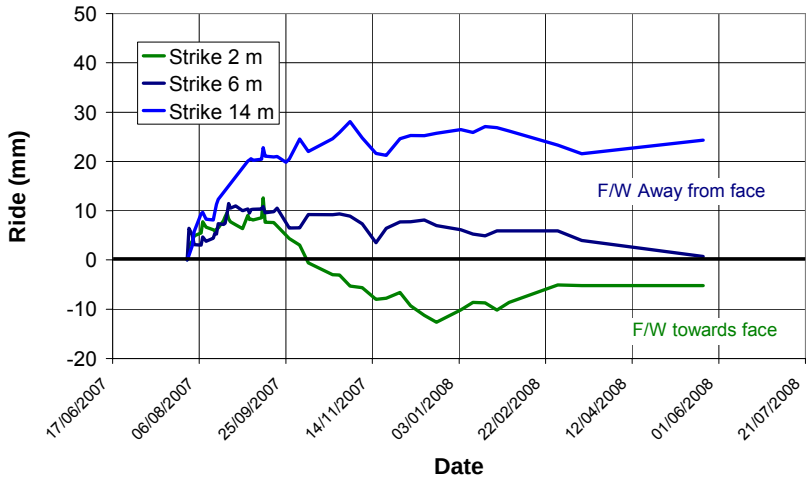

Figure E 21 Strike ride measurements in Panel 3S

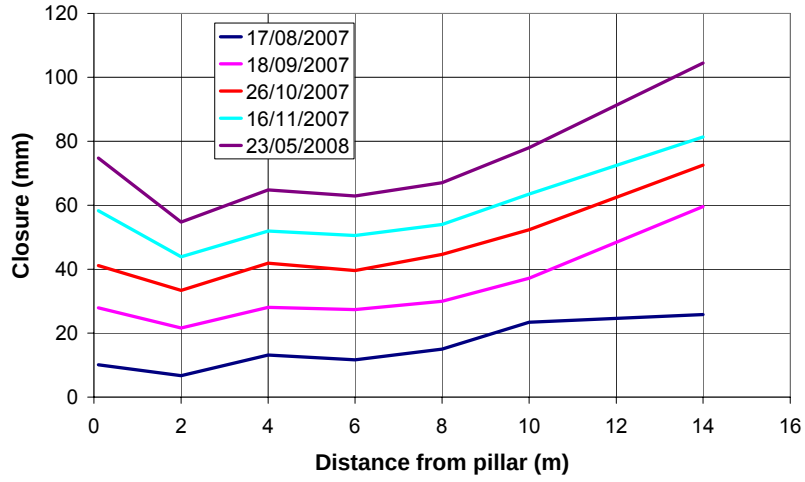

Figure E 22 Closure with distance from pillar edge

E2 Hangingwall investigations

E2.1 Introduction

The behaviour of the hangingwall was investigated using borehole camera surveys, extensometers and stress measurements. The results are compared to elastic models. Rock samples from horizontal and vertical boreholes were tested geomechanically and the results compared.

E2.2 Amandelbult 1-Shaft

E2.2.1 Location

Borehole V2 (Figure E 23) is a vertical hole drilled into the hangingwall and located one panel up from the closure measurements. The borehole was used for the stress measurements and the camera survey. Samples were also selected from every rock type and tested geomechanically. The face positions at the time of the stress measurements and the borehole camera survey is shown in Figure E 23.

Figure E 23 Stope sheet showing the vertical borehole (V2) drilled into the hangingwall at Amandelbult

E2.2.2 Borehole camera survey

The survey was conducted at the end of the instrumentation project, when all mining in the stope had been completed. Several possible horizontal fractures were identified up to about 1 m above the stope. However, the only definitely open fracture was observed at a height of 2.25 m above the stope (Figure E 24). A parting of between 2 mm and 5 mm appears to have developed at this height and there were also signs of what appeared to be borehole breakout here. No fracturing was observed above 2.25 m to a height of 15 m, which was the reach of the camera. The borehole was drilled through the base of the Bastard Reef some 20 m above the stope and the contact was intact in the core indicating that parting did not occur here.

Figure E 24 Open discontinuity at 2.25 m above the stope hangingwall

Shallow-dipping boreholes were drilled at the bottom of Panel 13-16-1E to determine the stress over two pillars spaced about 15 m apart. Water flowed from one borehole to another when the boreholes reached a vertical height of 2.7 m, suggesting an open discontinuity at this height above this panel. After some time water started to percolate through some of the vertical joints and roofbolts in the ASG. No water was observed in the panel below suggesting that the residual strength of the pillars was sufficient to close the discontinuities that were open above the stope. Approximately one year after stoping was completed, water was observed dripping from some of the vertical joints adjacent to the stability pillar in Panel 13-16-1E, which was not observed during the instrumentation programme. This suggests that some additional fracturing, not observed in the camera survey, had occurred in the hangingwall in the area of the high stress conditions above the stability pillar. However, the workings were still stable.

E2.2.3 Stress measurements

Triaxial stress measurements were conducted on either side of lithological boundaries (as defined by the mine geologist) in a vertical borehole (V2 in Figure E 23). Although no clear boundaries existed, the approximate heights and thickness of the strata are shown by the red dashed lines in Figure E 25 and Figure E 26. The stress results evaluated using biaxial tests performed on the original cells are shown in Table E 1 and Figure E 25. The measurements were also evaluated using the nonlinear-secant modulus method and these results are presented in Figure E 26. The two higher stress positions at 7 m and 16 m (Figure E 25) were associated with unreasonably high vertical stresses (Table E 1), which also corresponded to a higher degree of nonlinearity in the uniaxial test performed on cores immediately below the measurements (Figure E 27). The higher b-values are suspected to be the product of drilling under relatively high lateral stresses. The additional strain resulting from the opening of microcracks during drilling was subtracted out of the measured strains and the stresses re-evaluated. The results showed a slight drop in the higher stresses (Figure E 25) and more reasonable vertical stresses. However, the vertical stresses, which ranged between 2 MPa and 8 MPa, were much higher than the elastic model and some errors in the evaluation methodology are suspected.

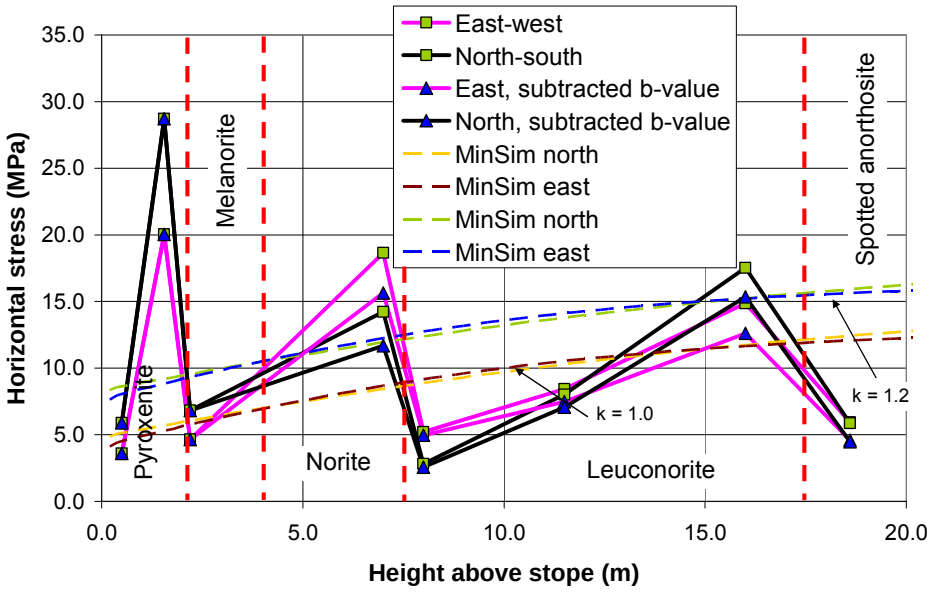

Figure E 25 Horizontal stresses in the North and East directions evaluated using biaxial test results, elastic model dotted

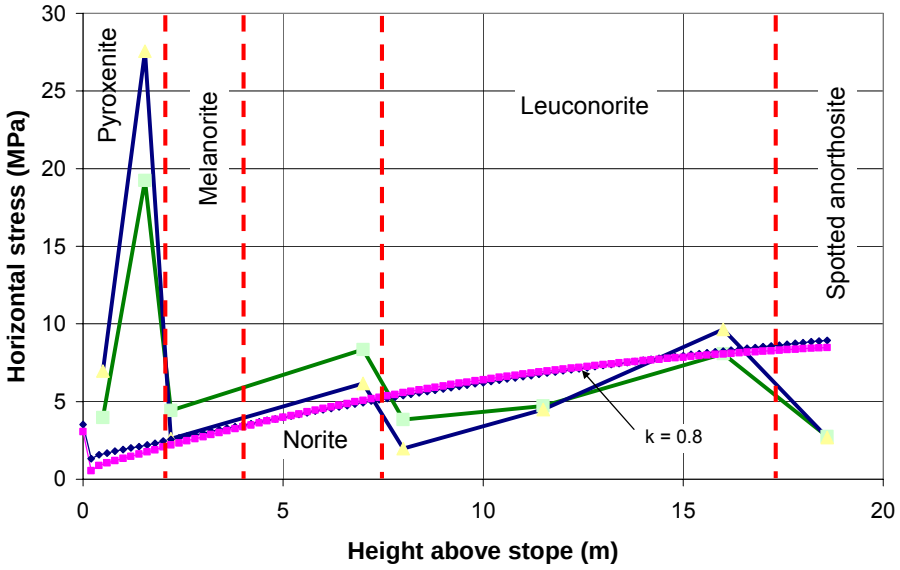

Figure E 26 Horizontal stresses in the North and East directions evaluated using the nonlinear evaluation technique, elastic model dotted

Table E 1 Results of the stress measurements performed in Borehole V2

Height (m)	Instrument type	North stress (MPa) X	East stress (MPa) Y	Vertical stress (MPa) Z
0.5	2D	5.9	3.6	-
1.6	3D	28.7	20.0	2.0
2.2	2D	6.8	4.6	-
7.0	3D	14.2	18.6	28.2
8.0	3D	2.8	5.2	6.6
11.5	3D	8.0	8.4	11.5
16.0	3D	17.5	14.8	26.9
18.6	3D	5.9	5.9	13.6

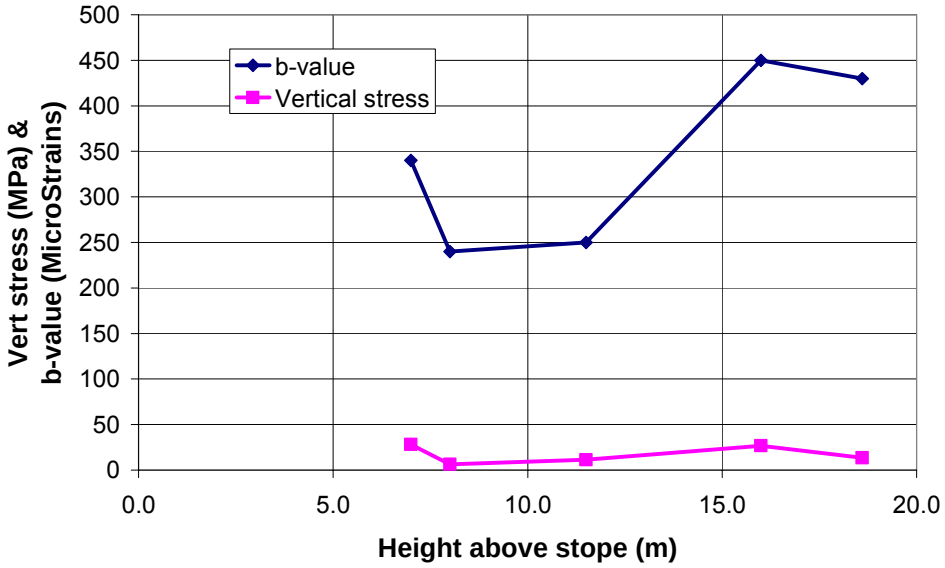

Figure E 27 Comparison between the measured vertical apparent stress (strain) and a measure of nonlinearity (b-value)

The difference in the two evaluation methodologies in Figure E 25 were small and suggest an overall k-ratio of about unity, which agrees with the blasthole socket dimensions and other stress measurements performed in the area. The profile of the measurements, however, suggests a series of beams in the hangingwall.

Only one possible beam surface was identified in the borehole camera survey at 2.3 m, which coincides with a change in rock type from pyroxenite to melanorite.

The nonlinear-secant modulus method of evaluating the stress measurements (Figure E 26) produced results that were closer to the MinSim model for a k-ratio of 0.8. However, this method is probably not appropriate at this site because the very small component of nonlinearity. The evaluation method applied in Figure E 25 appears more appropriate.

E2.3 Impala 10-shaft

E2.3.1 Location

The vertical and shallow dipping boreholes used to conduct borehole camera surveys, extensometer measurements and stress measurements in the hangingwall are shown in Figure E 28. The face positions at the time of the stress measurements conducted in boreholes V1a and V1b are shown in the figure. CSIRO1 was drilled ahead of the panels and the shallow-dipping boreholes were drilled when Panel 7s was an isolated panel and after mining had been completed in the stope.

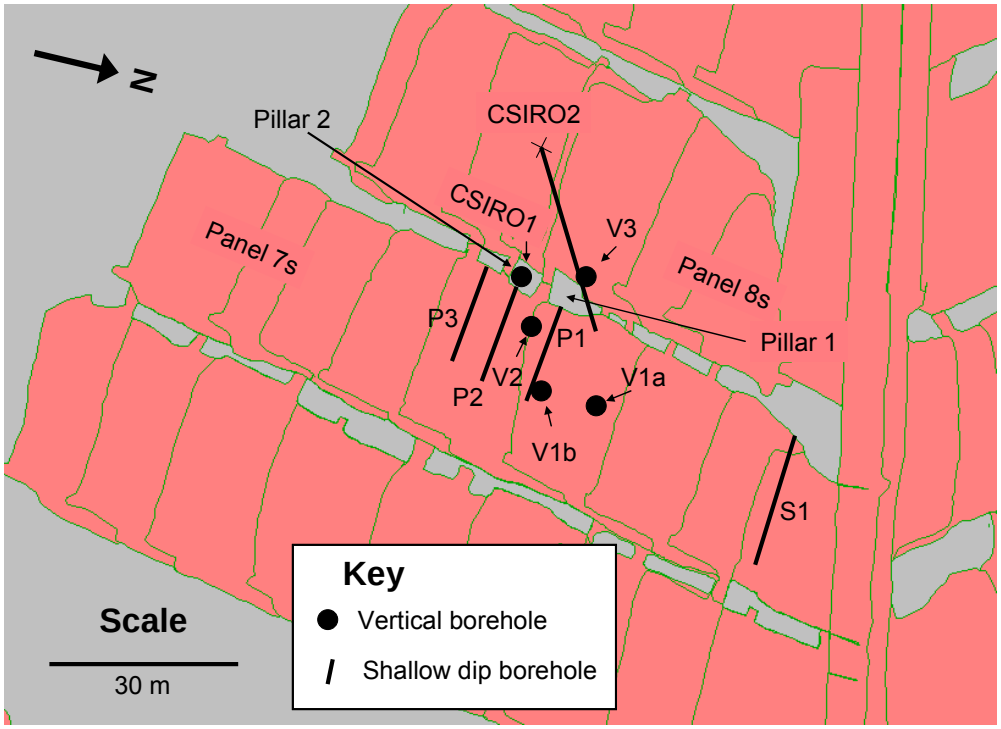

Figure E 28 Stope sheet showing the boreholes used to conduct stress measurements, borehole camera surveys and extensometer measurements

E2.3.2 Borehole camera survey

Borehole camera surveys were conducted in Boreholes V2 and V1a when the face positions were in the positions shown in Figure E 28. Boreholes V2 and V1a were located 5.5 m below the edge of the pillars and about in the centre of Panel 7s respectively. One shallow dipping discontinuity was observed 1.58 m above the hangingwall in V2, but evidence of movement or parting could not be positively identified. However, open discontinuities were evident up to a height above the stope of about 1.2 m during the drilling of a borehole parallel and adjacent to P1, as water was observed dripping from vertical joints up to 2 m from the pillar edge. An open discontinuity was also observed 0.23 m above the hangingwall in a vertical borehole about 1.5 m from Pillar 2. Open discontinuities were not observed in V1a and the weak parting plane at the base of the Bastard reef some 12 m above the stope was intact in both boreholes. The core from V2

(Figure E 29) also showed a solid contact at the base of the Bastard reef and apart from some small pieces in the first 0.5 m there was no clear evidence of fracturing.

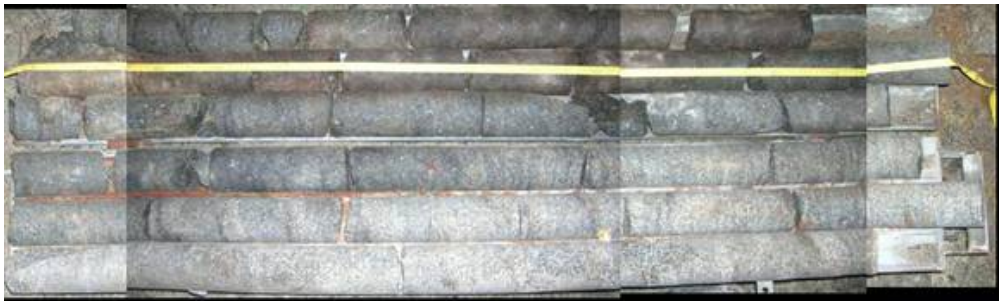

Figure E 29 Core from V2

Four 15 m to 20 m long boreholes were drilled 10° to 20° steeper than the strata in Panel 7s ahead of the up-dip and down-dip panels to install doorstopper stress cells. These holes were wide spread across the panel as shown in Figure E 28. The core of each one was inspected for evidence of fractures. Shallow dipping fractures should have been easy to observe if present. However, no fractures could be positively identified. A further three shallow-dipping and one vertical boreholes were drilled adjacent to P1, P2 and P3 and V1a respectively after the 8s face reached its final position and the 6s and 7s faces were in the positions shown in Figure E 28. No evidence of fracturing was found in the cores of these boreholes either.

E2.3.3 Extensometer results

Three extensometers were installed in the hangingwall to measure horizontal and vertical deformations. A vertical extensometer was installed through the centre of Pillar 2 (CSIRO1 in Figure E 28) ahead of the up-dip and down-dip panels and measured the vertical deformation that occurred between the top of the pillar and 4.18 m above the pillar (Figure E 30). Positive deformation represents compression. Pillar failure occurred about 1 m ahead of the lagging up-dip face and the deformation up to failure initiation was shown to be elastic (Figure E 30), using the ‘matrix’ constants for spotted anorthosite. After failure initiation, the elastic deformations were followed by significant inelastic compressive

deformations before the borehole was sheared. These results suggest that the pillar was punching into the hangingwall. The tensile deformations that occurred after pillar failure may have been the result of borehole shearing or relaxing of the strata. The compressive measurements that occurred after shearing are likely to represent at least some of the hangingwall punching that occurred at the centre of the pillar. The flattening of the curve at 11 m face advance in Figure E 30 coincided with the beginning of the steady state residual strength shown by the pillar stress measurements. However, all hangingwall deformations measured after pillar failure are suspect as the hole appears to have sheared during pillar failure.

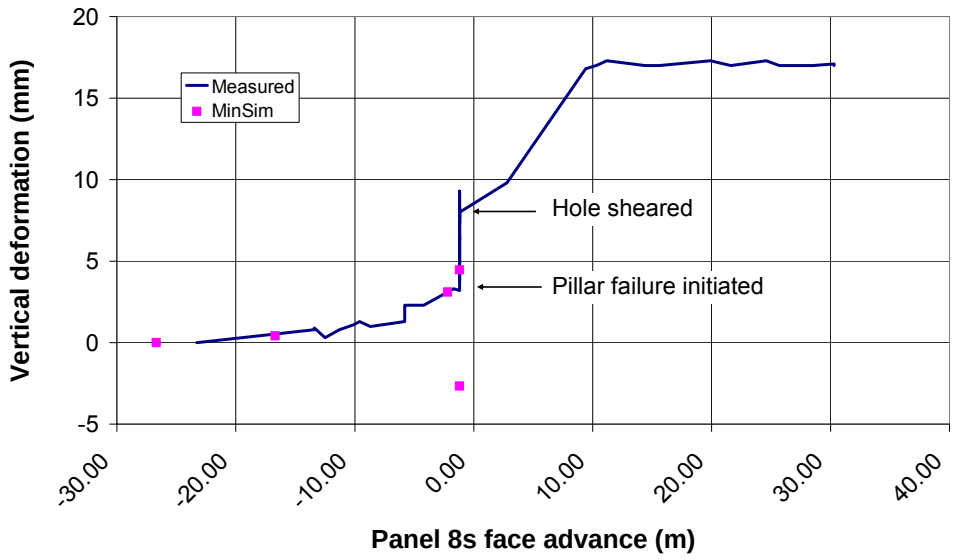

Figure E 30 Hangingwall deformations above the centre of Pillar 2, between the pillar top contact and 4.18 m above the Pillar. Elastic E = 83 GPa and v = 0.32

An extensometer was also installed in a vertical borehole located about 5.5 m down-dip of Pillar 2 (V2 in Figure E 28) and measured deformation between the stope hangingwall and a point 0.6 m above the base of the Bastard Reef. Unfortunately the extensometer was only installed on 2 August 2006, well behind the 6s and 7s faces and after the 8s face had reached its final position. Very little deformation was measured (Figure E 31) indicating that little or no foundation failure occurred since the extensometer was installed and no parting occurred on

the Bastard Reef contact (the extensometer has an accuracy of about 0.5 mm and the measured deformation may have been due to instrumental errors).

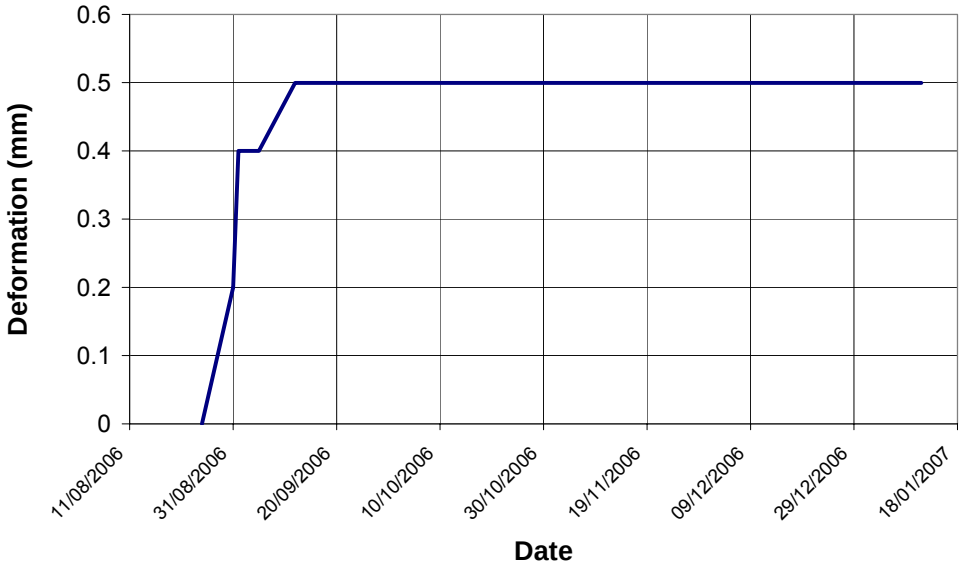

Figure E 31 Deformation measured between the stope hangingwall and the Bastard Reef, a vertical height of 12.8 m, in Borehole V2

An extensometer was installed in CSIRO2 (Figure E 28) to measure the horizontal deformations in the hangingwall over a pillar and stope during mining. The deformations that took place ahead of the Panel 8s face were elastic (Figure E 32). However, once pillar failure occurred (about 2 m behind the face), significant inelastic deformations were observed over the pillar (Figure E 32) and the stope (Figure E 33). The negative inelastic deformations that occurred over the pillar are suspected to be the result of failure due to pillar punching. The "inelastic" deformations between the pillar and the centre of the panel (Figure E 33) are positive, which means that the reference points moved closer to one another. This suggests an induced compressive stress in the horizontal direction, probably as a result of pillar punching; or possibly some not well understood strain effects during the opening of microfractures (as the vertical stress was relaxed). Further evidence of stress induction due to pillar punching was provided by stress measurements that were conducted just ahead of the extensometer reference points. These measurements are described in the following section.

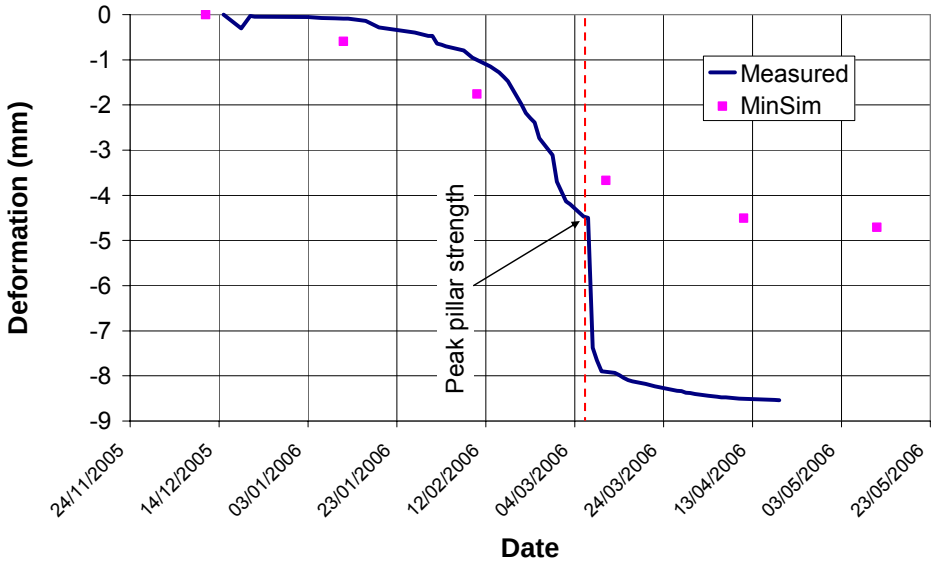

Figure E 32 Horizontal deformation in the hangingwall across the top of a pillar. Measurements performed in Borehole CSIRO2

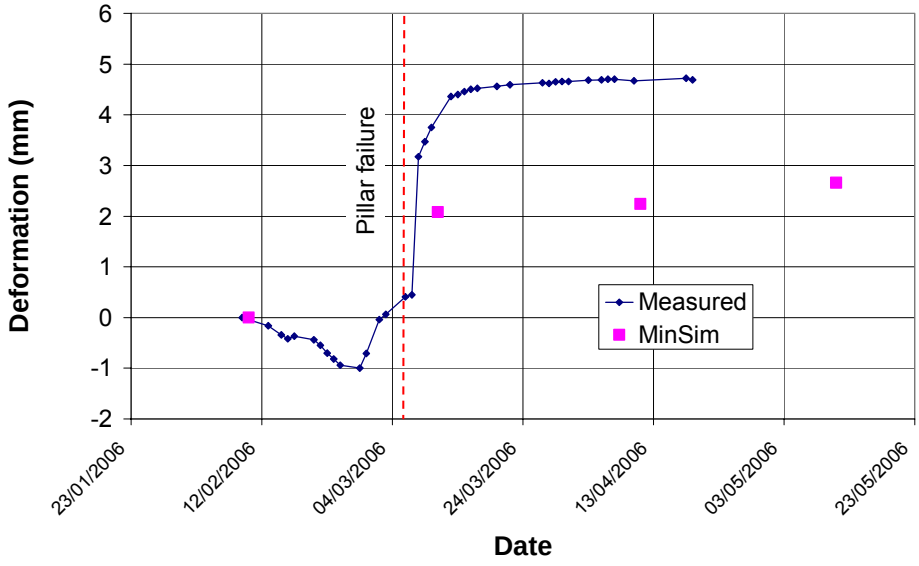

Figure E 33 Horizontal deformation in the hangingwall across a panel at vertical heights between 1.5 m and 5.5 m above the stope. Measurements performed in Borehole CSIRO2

E2.3.4 Stress measurements

Measurements were conducted over Panel 8s in Borehole CSIRO2 to determine the stress change in the hangingwall during the mining of this panel. The vertical stress results are provided as a function of face advance and compared to an elastic model in Figure E 34. The good correlation between the measurements and the elastic model up to a face advance of about 8 m confirms the matrix elastic constants used in the evaluation of the stress measurements. Good comparisons between the extensometers and elastic models were also achieved during elastic loading conditions when these constants were applied to the models.

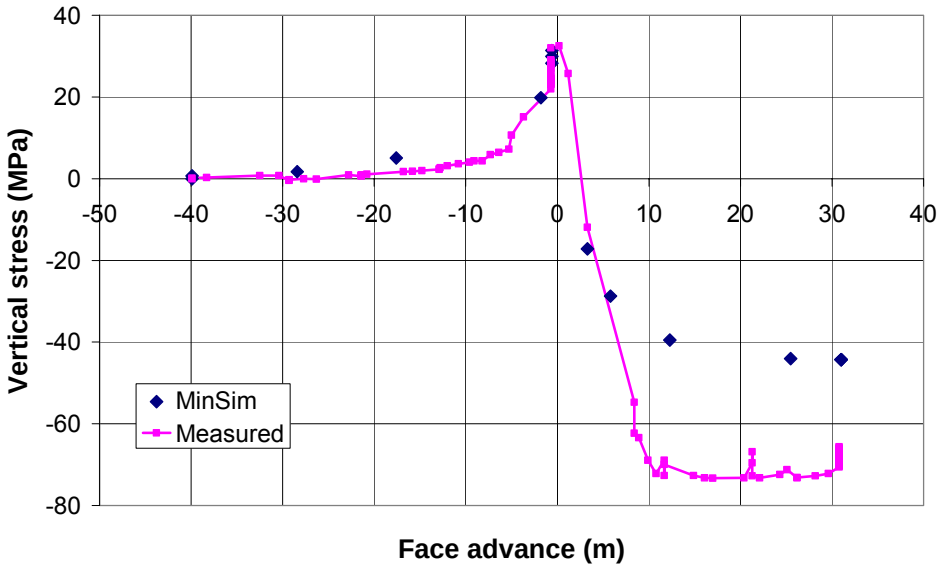

Figure E 34 Vertical stress change 4.7 m above the centre of Panel 8s in Borehole CSIRO2. Negative face positions are behind the cell

The match between the horizontal stress in the strike direction (North) is less convincing than the vertical correlation (Figure E 35). A 2D DIGS model (Napier and Hildyard, 1992) was run to observe the possible effects of beam development on horizontal stress. The model showed that high horizontal stresses can be generated near the front of a fracture that develops with the face advance due to the induced shear stresses. The profile shown in Figure E 35 is described if such a parting develops just below the measurement point.

Unfortunately no camera surveys were conducted in Panel 8s and therefore the existence of such a plane cannot be verified. The panel was, however, prematurely stopped due to poor hangingwall conditions and fracturing at the face.

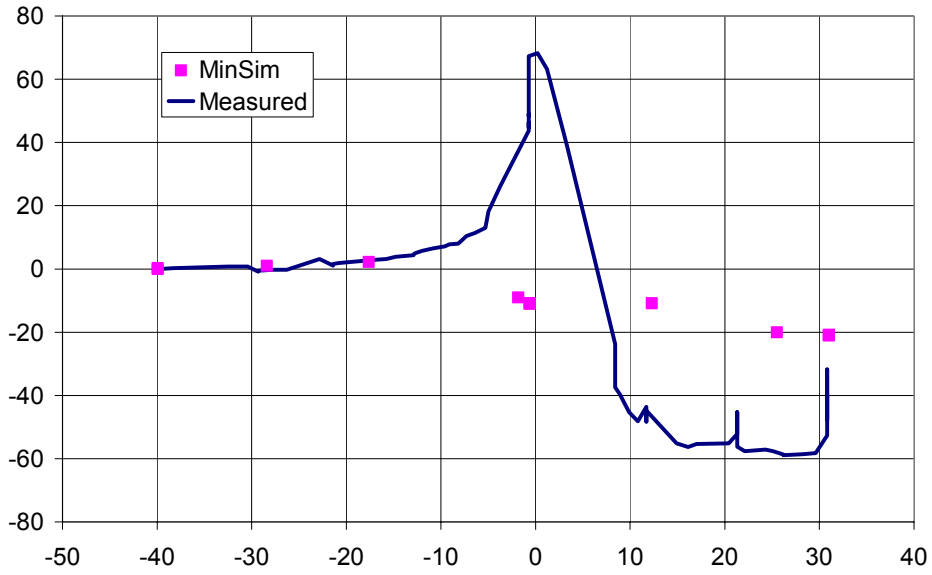

Figure E 35 Horizontal stress change in the strike direction, 4.7 m above the centre of Panel 8s in Borehole CSIRO2. Negative face positions are behind the cell

If the advancing fracture and associated shear stress is the reason for the relatively high horizontal stress measured in the strike direction, the stress change in the dip direction would not be directly affected by the assumed shear stress. However, there is a Poisson effect that could explain the higher measured than modelled stresses shown in Figure E 36. The reason for the relatively small drop after the peak stress is not understood. However, the slopes of the unload portion of the measured and modelled curves are similar.

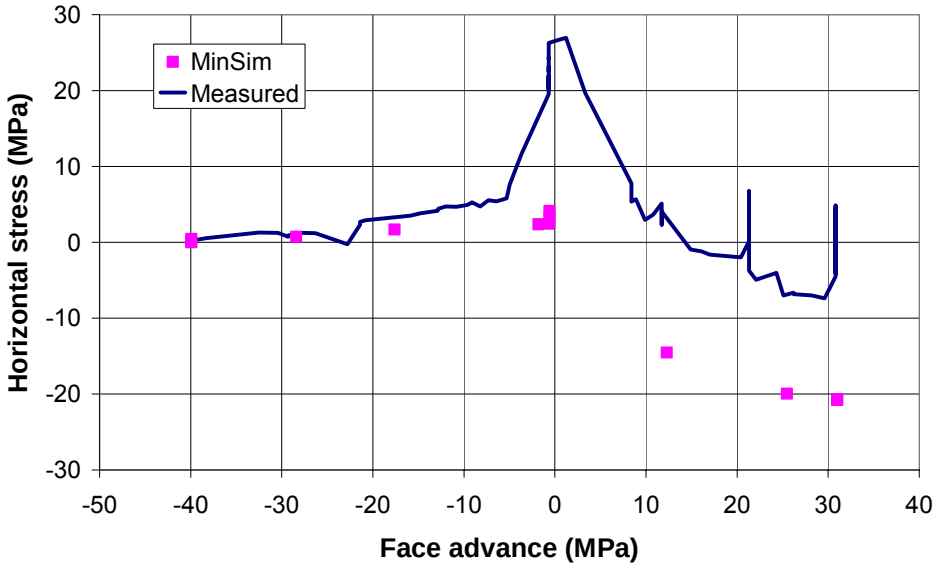

Figure E 36 Horizontal stress change in the dip direction, 4.7 m above the centre of Panel 8s in Borehole CSIRO2. Negative face positions are behind the cell

Stress change measurements were also conducted in the hangingwall over three pillars in Boreholes: CSIRO1, P1 and P3. The pre-failure vertical stresses are shown in Figure E 37, Figure E 38 and Figure E 39. In every case there is a reasonably good correlation with the elastic models when the measurements were evaluated using the matrix elastic modulii of the rock in which the cells were located. The horizontal stresses measured on the down-dip side of the pillars (P1 and P2) also correlated well with elastic models (Figure E 40 and Figure E 41). However, this was not true of the measurements in Borehole CSIRO1 (Figure E 42). A better match was achieved when the measurements were compared to modelled stresses that were closer to the pillar. The horizontal stress at this position appears to be sensitive to the stress condition of adjacent pillars and the mismatch may be an artefact of incorrectly assigning these stresses in the model. The stress condition over the pillar may also have been affected by vertical discontinuities and fractures as shown by the stress channelling effects of these discontinuities in an ELFEN model (Figure E 43). Vertical stress fractures were observed in shallow dipping boreholes drilled closer than 1.2 m above the pillars, but no evidence of stress fractures were found higher than this.

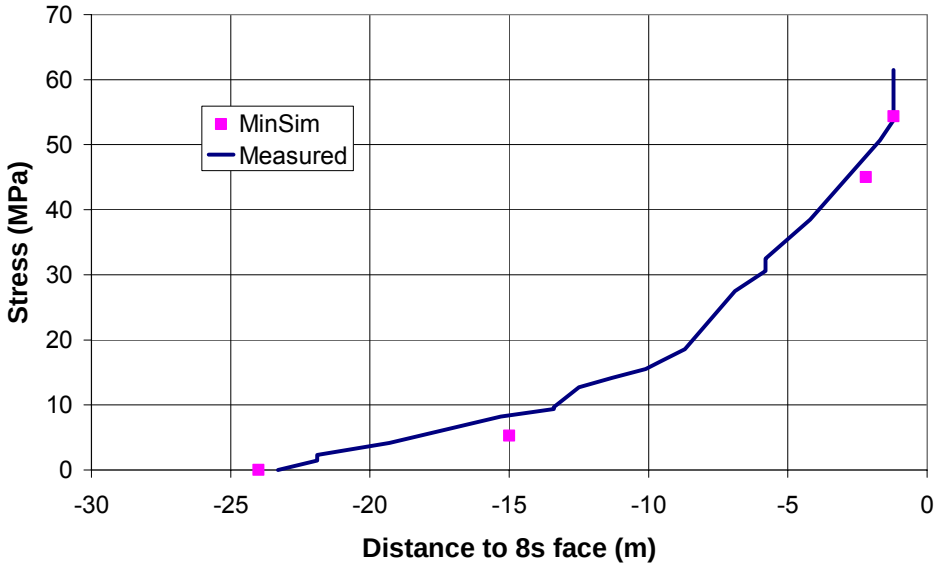

Figure E 37 Vertical stress change 4.2 m above Pillar 2 in Borehole CSIRO1. Negative face positions are behind the cell

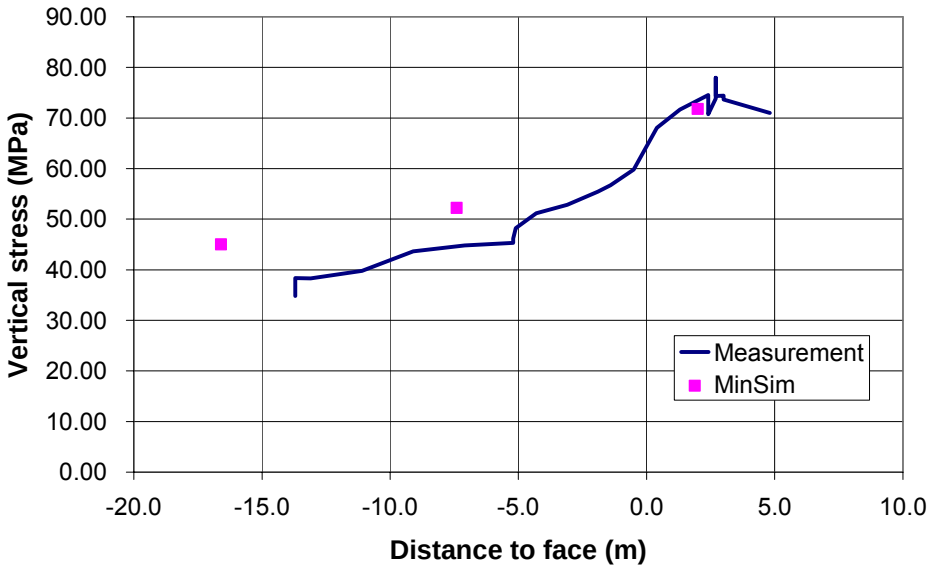

Figure E 38 Vertical stress change 5.28 m above the pillar in Borehole P1. Negative face positions are behind the cell

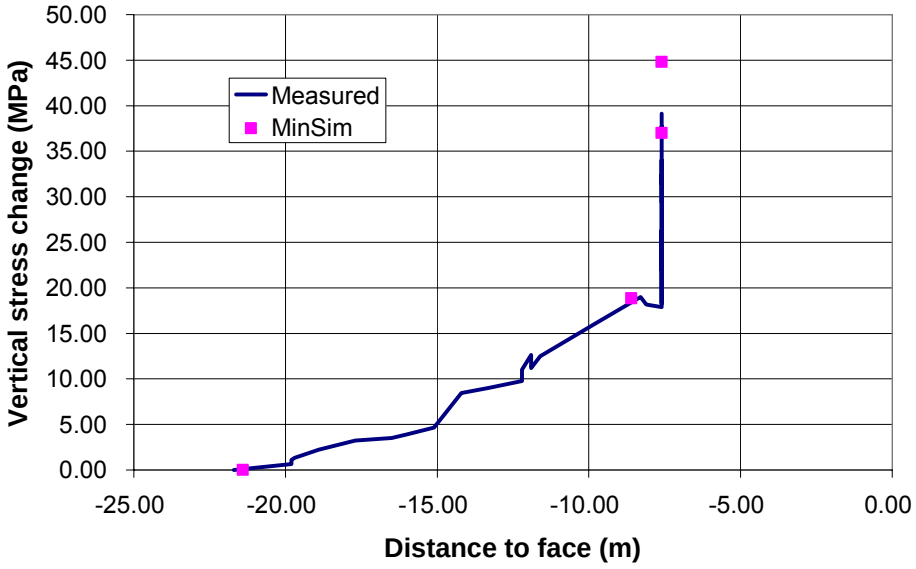

Figure E 39 Vertical stress change 3.23 m above the pillar in Borehole P3. Negative face positions are behind the cell

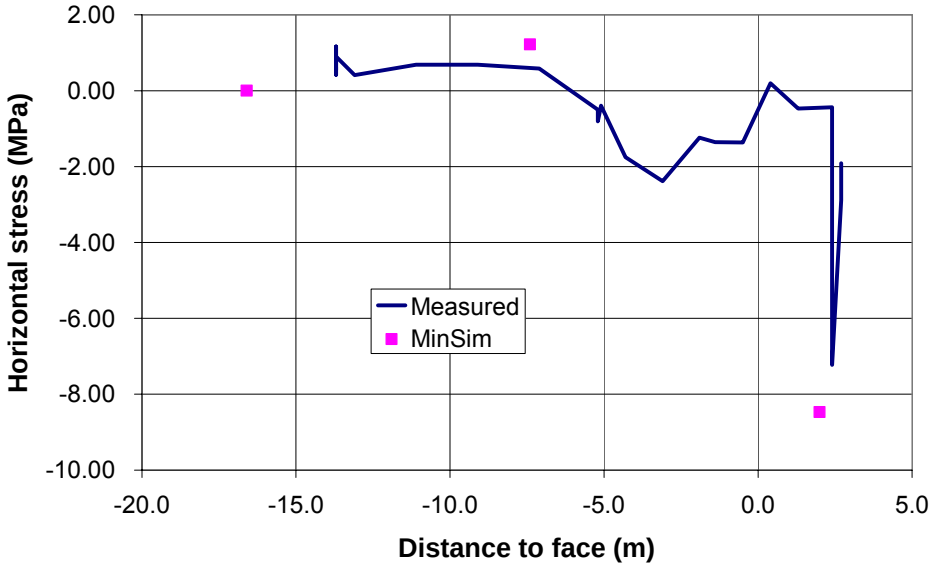

Figure E 40 Horizontal stress change in the strike direction, 5.28 m above the pillar in Borehole P1. Negative face positions are behind the cell

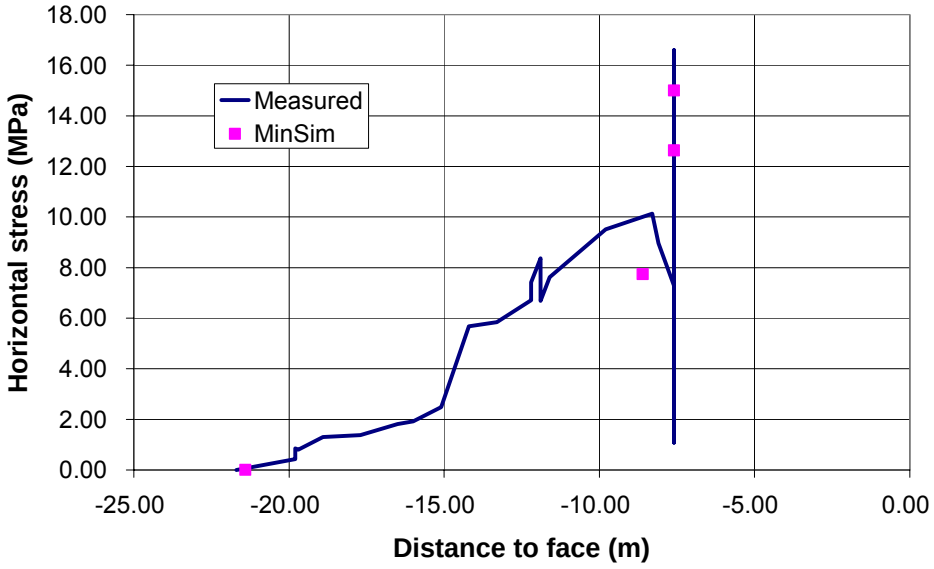

Figure E 41 Horizontal stress change in the strike direction, 3.23 m above the pillar in Borehole P3. Negative face positions are behind the cell

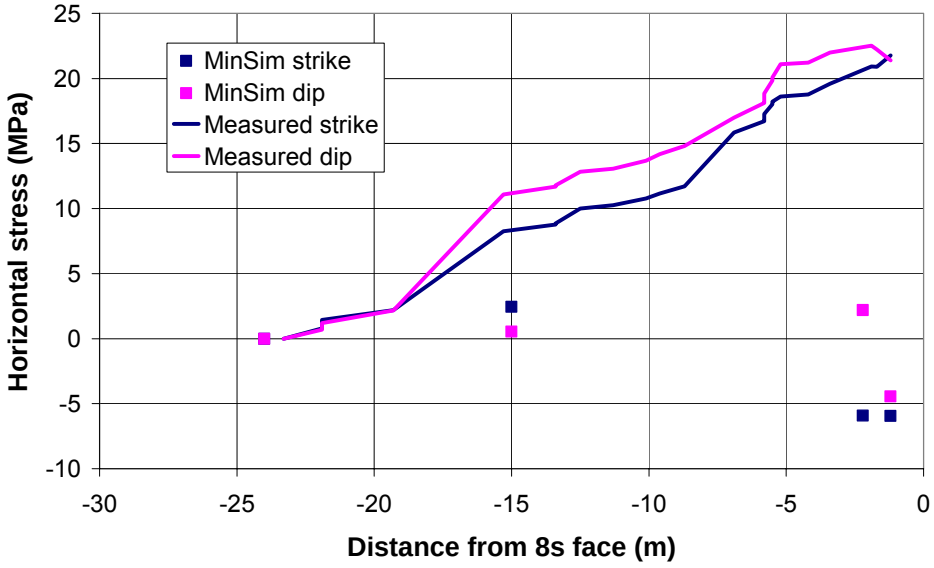

Figure E 42 Horizontal stress change 4.2 m above Pillar 2 in Borehole CSIRO1. Negative face positions are behind the cell

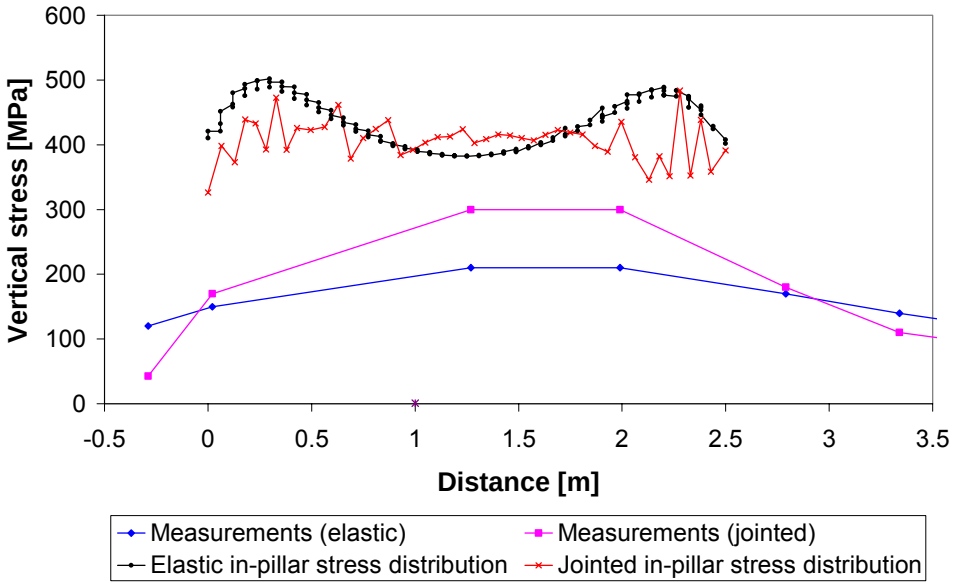

Figure E 43 ELFEN model showing the effects of 1.2 m long vertical fractures above a pillar (jointed) on the measured stress about 2.5 m above a pillar

A series of horizontal stress measurements were conducted in two vertical Boreholes V1a and V1b using doorstopper strain cells. Borehole V1a was located in a small pothole, where the first measurement was conducted in leuconorite and the other measurements were all conducted in spotted and mottled anorthosites except for the measurement in the Bastard Reef pyroxenite at 12.2 m above the stope. The second set of measurements were conducted about 10 m from the pothole (V1b) and the first two measurements were conducted in the normal pyroxenite and melanorite rock types. The stress results of the two boreholes are provided in Figure E 44. The two boreholes showed different stress conditions up to a height about 3 m above the stope, but above this height the results showed the same trend with only minor differences. The peak stresses at 6 m and 10 m in Borehole V1a (Pothole) coincided with a pink spotted and mottled anothosite respectively. This pink colouration in the anorthosites is unusual on the mine and has only been observed in potholes, where iron enrichment has taken place (Jenkinson, 2006). The drop in stress at 8 m in Borehole V1a occurred where the rock changed from pink to white spotted anorthosite. No pink anorthosite was observed in Borehole V1b. The good correlation between the measurements in the two boreholes above 3 m suggests

that there was little influence of the pothole on the hangingwall conditions above this height. The shaft geologist confirmed that that this was usually true for small potholes in the area (Jenkinson, 2006).

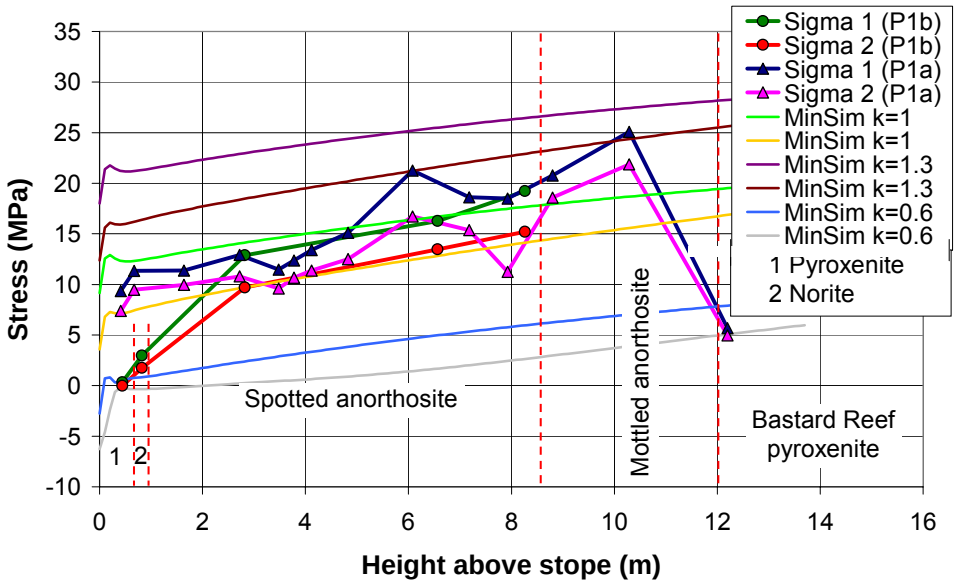

Figure E 44 Horizontal stress with height above the stope. The models assumed 30 MPa for the pillar residual strength

The elastic model that best fit the measurements assumed a pillar residual strength of 30 MPa and a k-ratio of unity (Figure E 44). Higher residual strengths increased the slope while the k-ratio governed the magnitude. The measured results in Borehole V1a were higher than the model with a k-ratio of unity where pink anorthosites were observed. A better fit was obtained when a k-ratio of 1.3 was assumed for these rock types (6 m, and 10 m above the stope). The darker rocks (pyroxenites and norites) showed a lower stress than predicted by the model with a k-ratio of unity. The Bastard Reef pyroxenites suggest that a k-ratio of about 0.6 is more applicable to this rock type. The measurements, therefore, indicate some sort of stress “channelling” with the lighter coloured rocks carrying higher horizontal stresses than the darker rocks. These stresses may be tectonic and further investigations should be made to better understand the rock mass behaviour. The modelled k-ratio may not be the in situ stress condition as the

horizontal stress dropped below the elastic levels in the stress change measurements conducted in Panel 8s (CSIRO2).

E2.4 Union Spud shaft

E2.4.1 Location

The hangingwall behaviour was studied at two sites (Figure E 45 and Figure E 46). Vertical boreholes were provided for borehole camera surveys, extensometers and stress measurements.

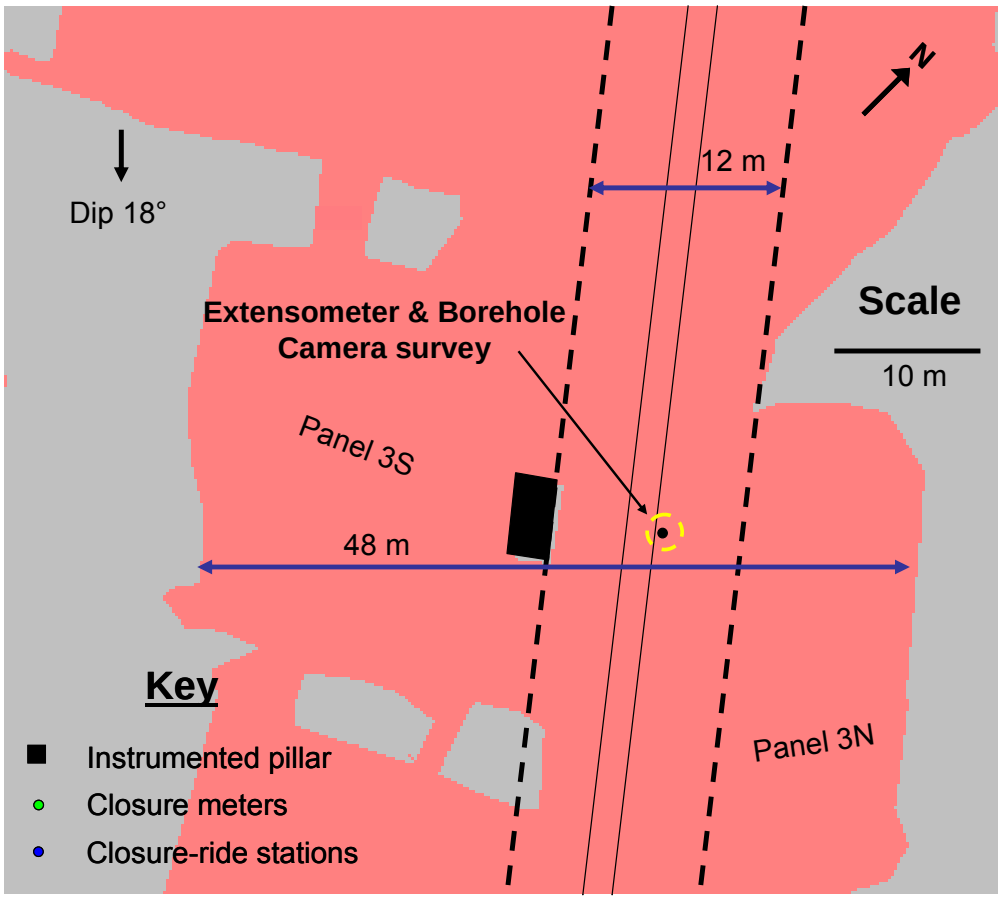

Figure E 45 Vertical boreholes used for extensometers and borehole camera surveys

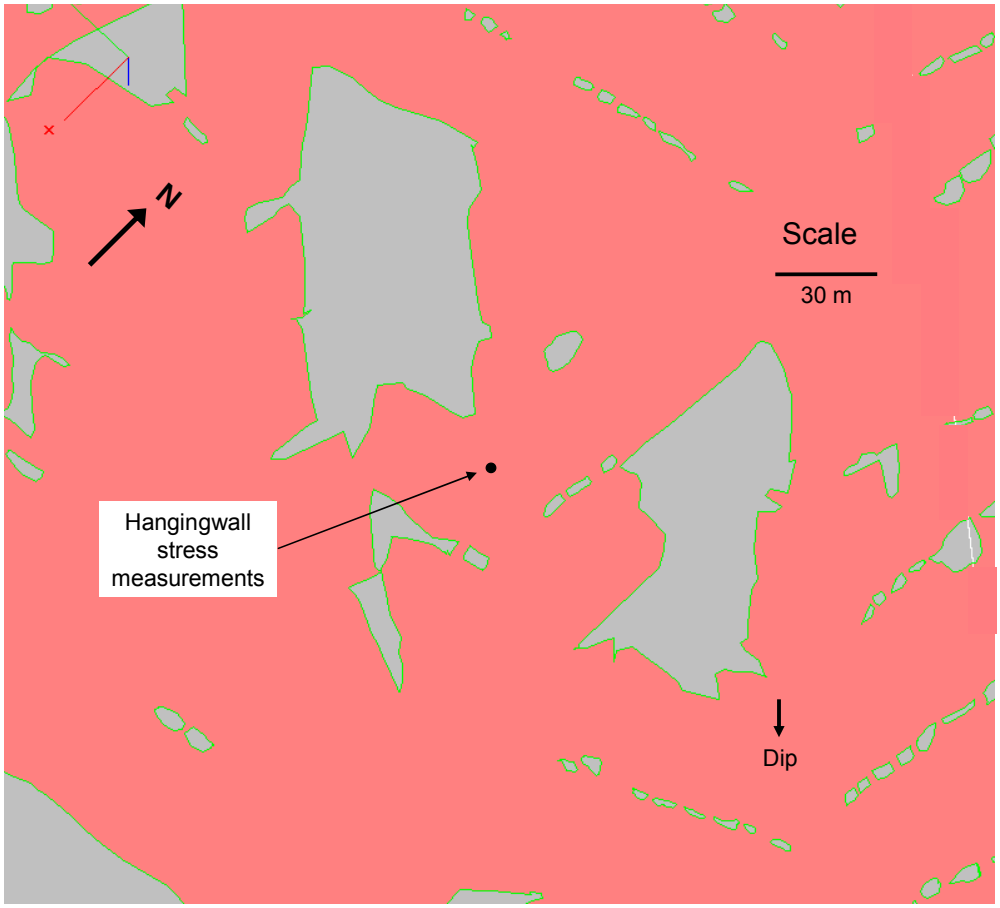

Figure E 46 Stope sheet showing the location of the horizontal stress measurements conducted in a vertical borehole drilled into the hangingwall at Union Spud shaft

E2.4.2 Borehole camera surveys

Borehole camera surveys were conducted in a hole adjacent to the extensometer (Figure E 45) before and after Panels 3S and 3N had been mined. The initial survey was conducted after the raise had been ledged as shown by the dashed lines in Figure E 45. The strike span across the ledged raise was 12 m. The results of the investigation are compared to a survey conducted after the panels were complete in Table E 2. The strike span across the stope from the south face in Panel 3S to the north face in Panel 3N was about 48 m (Figure E 45) when the second survey was done (the pillar in Panel 3S crushed and was carrying a small

load at the time of the second survey). At a span of 12 m, the highest open shallow dipping discontinuity was 3.22 m above the stope. A few steeply dipping open joints were observed up to a height of 10.0 m. All of these discontinuities were open by small amounts and it is possible that the filling of existing joints were washed out during the drilling, giving the appearance of being open. The chromitite at the base of the Bastard Reef (19.93 m) appeared cracked, but it could not be determined if the cracks were geological or as a result of mining. Table E 2 shows that after the panels had been mined there were significantly more open discontinuities than in the narrow span and the height to the top of the open fractures also increased to 12.8 m above the stope. Significant discontinuity apertures were also observed, extending up to a height of about 5 m above the stope, after the panels had been mined.

Table E 2 Results of the borehole camera surveys conducted in the hangingwall of Panel 3N (Figure E 45)

At ledging stage			After Panels 3S and 3N mined		
Height (m)	Orientation (Degrees)	Aperture (mm)	Height (m)	Orientation (Degrees)	Aperture (mm)
0.52	**0**	**1**	**0.5**	**0**	**3.0**
0.82	80	1	1.17	90	1.0
1.07	70	1	2.1	80	1.0
1.12	80	1	**2.59**	**10**	**8.0**
1.67	80	1	**2.74**	**20**	**5.0**
3.22	**20**	**0.5**	**2.80**	**20**	**0.5**
6.92	80	0.5	3.10	80	0.5
10.42	80	0.5	**3.16**	**20**	**0.5**
20.35	**20**	**0.1**	**3.40**	**20**	**3.0**
			3.68	80	1.0
			4.61	80	2.0
			4.75	**20**	**0.5**
			5.15	**20**	**1.0**
			5.75	80	0.5
			6.33	80	0.5
			7.55	**20**	**0.5**
			9.03	**20**	**0.5**
			11.05	80	0.5
			12.8	**20**	**0.5**
			20.35	**20**	**0.1**

Yellow = pyroxenite; Tan = norite; Green = leuconorite; Blue = Bastard Reef contact; Shallow-dipping discontinuities in bold.

The additional open discontinuities observed after the panels had been mined show that inelastic deformations occurred in the hangingwall. Some of the shallow-dipping discontinuities may have been fractures as these discontinuities were not observed during the first survey and such fractures have been observed

in other investigations at Union Section (Watson, 1996). No open fractures were observed between 13 m and 20 m above the stope and the Bastard Reef contact appeared in the same condition as in the first survey (before mining the panels).

The results of the borehole camera survey conducted in the stress measurement borehole (Figure E 46) are shown in Table E 3. All mining had been completed in the area at the time of the survey. Shallow-dipping discontinuities were open with significant apertures to a height of 5.63 m above the stope and signs of possible movement were observed at the base of the Bastard Reef at 26.75 m above the stope (Figure E 47). The open joint at 27.15 m (Table E 3) provides further evidence of movement on the Bastard Reef contact. A distinct change in rock type from norite to leuconorite was observed at a height of 6.13 m and the observed parting at 5.63 m is suspected to be associated with this plane. A change from leuconorite to spotted anorthosite occurred at about 19.75 m. No obviously open discontinuities were observed between 10.6 m and the base of the Bastard Reef (26.75 m).

Table E 3 Results of the borehole camera surveys conducted in the stress measurement hole (Figure E 46)

Height (m)	Orientation (Degrees)	Aperture (mm)
0.1	10	1.0
1.15	10	5.0
1.23	90	3.0
1.50	20	5.0
3.50	20	0.5
3.67	20	2.0
5.08	80	0.5
5.30	0	2.0
5.38	0	0.5
5.63	20	2
6.30	80	0.5
6.58	80	0.5
6.90	80	0.5
7.48	80	0.5
10.60	20	0.2
26.75	20	0.3
27.15	80	2.0

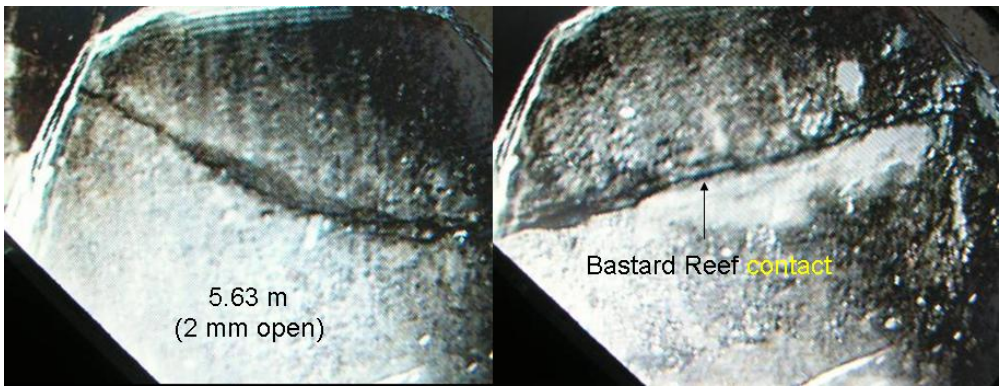

Figure E 47 Open discontiuities at 5.63 m above the stope and at the base of the Bastard Reef. The opening on the Bastard Reef contact may have been an illusion created by the drilling process, i.e. chipping of the contact

The core from the extensometer borehole in Figure E 45 is shown in Figure E 48. Significantly more jointing was observed in the pyroxenites and darker norites immediately above the stope than in the lighter norites higher up in the sequence. No jointing was observed in the upper 5 m section of the leuconorites. Mainly sub-vertical jointing was observed in the anorthosites above the solid leuconorite and several different joint angles were identified in the Bastard pyroxenites. A serpentinite-filled strata-parallel discontinuity was observed in the contact at the base of the Bastard Reef.

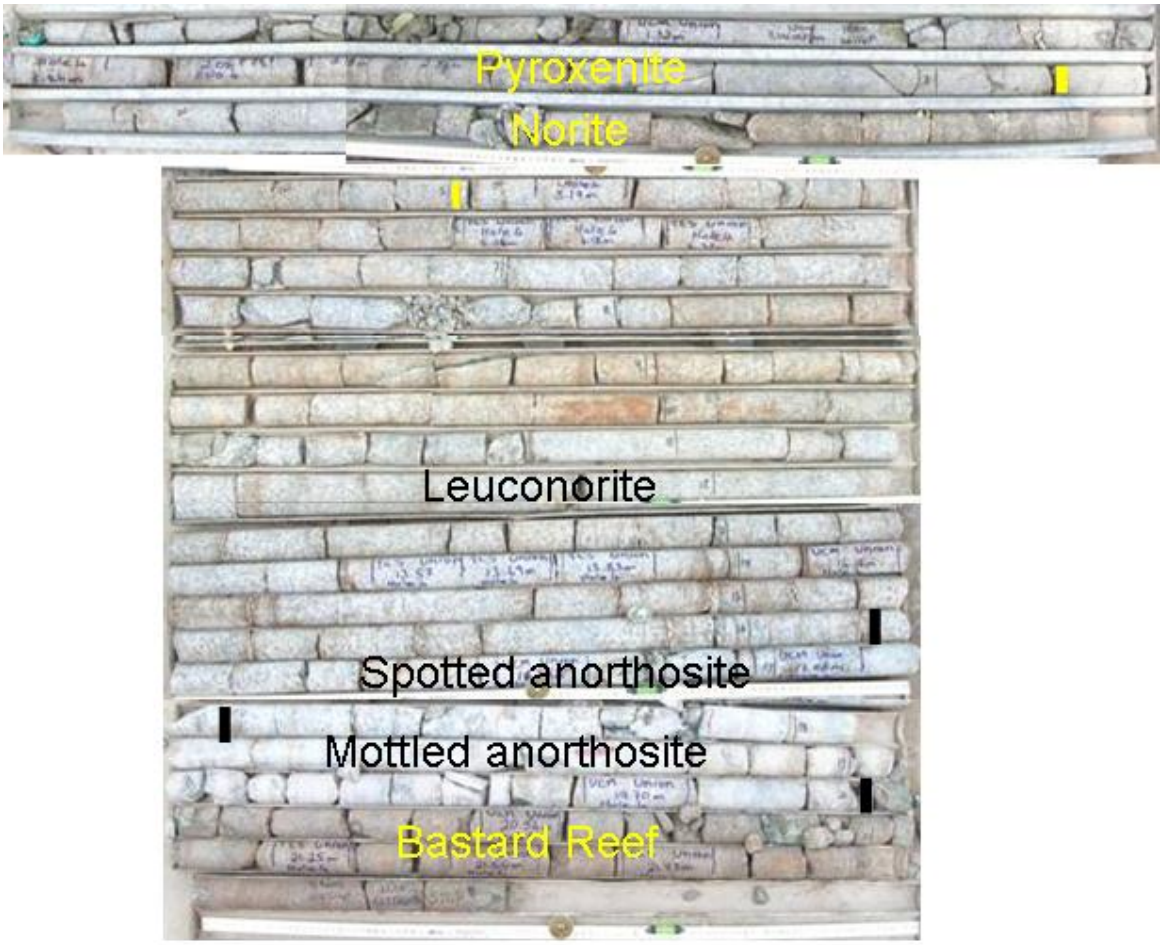

Figure E 48 Borehole core from the hangingwall extensometer hole (Figure E 45). The top tray is 1.5 m long and the others are 1 m long

E2.4.3 Extensometer results

A single anchor extensometer was installed in a vertical borehole to measure the deformations that occurred in the hangingwall up to 21 m above the stope. The anchor was installed above the base of the Bastard Reef to include any inelastic deformations that may occur at this point. The borehole was drilled from a cubby located off the centre gully, in Panel 3N, 6.3 m from the edge of the instrumented pillar when the ledge span was 12 m as shown in Figure E 45. Deformations were measured for a period of 14 months, which included all the mining in the stope, and the results of the investigation are shown in Figure E 49. The comparison between the measurements and the elastic results suggest that significant inelastic deformation took place during the monitoring period. The 60 GPa Young's modulus used in the model was already significantly lower than the laboratory results, but since this modulus provided reasonable agreement to the measurements in the narrow (12 m) span conditions, it was assumed as the rock mass modulus. An average Poisson's Ratio of about 0.32 was determined from the test laboratory.

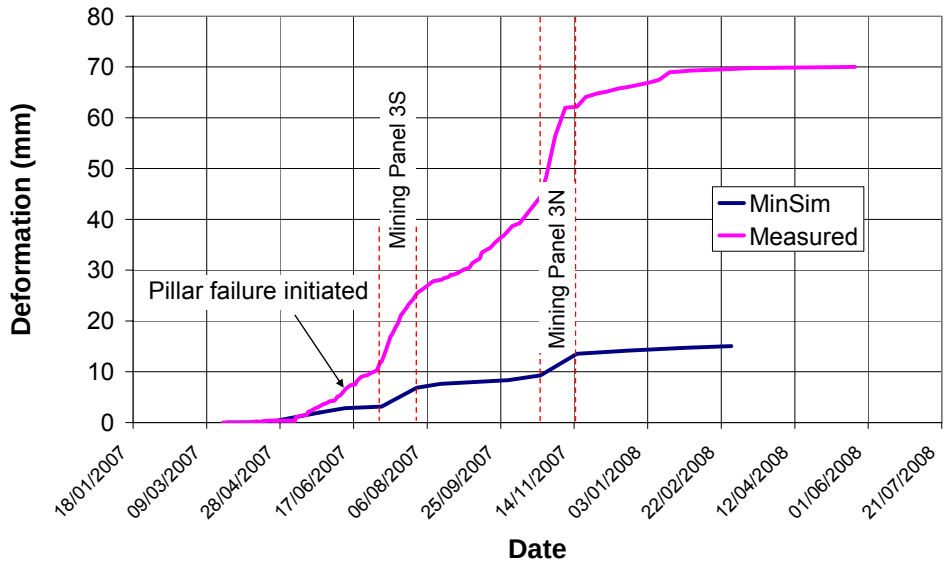

Figure E 49 Union Spud shaft hangingwall extensometer results. The elastic model assumes E = 60GPa and v = 0.32

Pillar failure was gradual and since the face was close to the pillar at the time of failure there was little obvious impact of this failure on the results. The effects of hangingwall pillar punching were not observed in the area of the extensometer and therefore the increased deformation rate measured during the period of mining in Panel 3S (Figure E 49) are assumed to be the effects of the increasing span on the other side of the crushed pillar. A similar profile was observed when mining took place in Panel 3N.

E2.4.4 Stress measurements

Stress change measurements were conducted 5.3 m over the instrumented pillar and 3.3 m above the stope (0.5 m from the pillar edge). The results of the vertical measurements have been compared to elastic models in Figure E 50 and Figure E 51. The measurements over the pillar compared favourably with the elastic model up to 18 April 2007. At this stage the proposed pillar was exposed on the up-dip side but no mining had occurred on the down-dip side. The mining of the face on the down-dip side of the proposed pillar resulted in higher stresses than predicted by the model. These stresses are suspected to be the result of fracturing on the pillar sidewall, resulting in the peak stress being closer to the cell than predicted by the elastic model. The sidewall fracturing is also suspected to be the reason for the poor correlation of the measurements to the elastic model in Figure E 51. As the measurements were conducted away from the edge of the pillar, fracture propagation into the pillar resulted in the peak stress moving away from the measurement position.

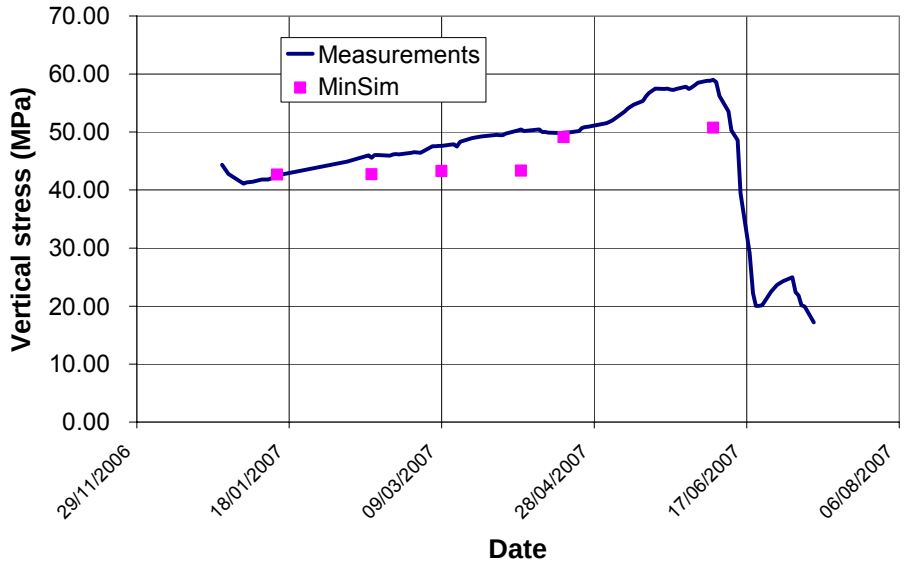

Figure E 50 Vertical stress change measurements at 5.3 m above the centre of the instrumented pillar (P1b in Figure E 45)

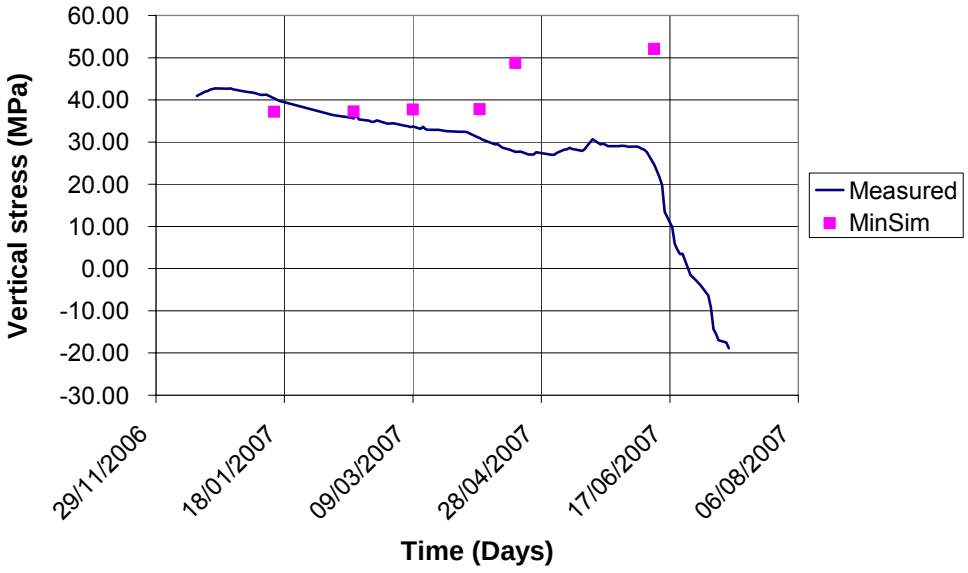

Figure E 51 Stress change measurements at 3.3 m above the hangingwall and 0.5 m horizontally from the instrumented pillar (P1a in Figure E 45)

The measured stresses in Figure E 51 were compared to the predicted elastic stresses along the borehole direction. The distances from the original toe of the borehole were assumed to represent the distance that the peak stress had moved from the original sidewall position. These back-analysed distances were assumed to be a crude measure of the depth of fracturing and plotted against the pillar stress in Figure E 52. The analysis suggests that this fracturing initiated at an APS of 82 MPa. MinSim indicates that the sidewall stress may have been as much as 170 MPa at this stress. Figure E 52 suggests that the depth of fracturing may have been a linear function of APS. If the back-analysis in Figure E 52 is a true reflection on the depth of fracturing, the results suggests that fracturing propagated at least half-way through the pillar and therefore the final pillar was fractured throughout. These results, therefore, suggest that a 2.8 m wide pillar in a stoping width of about 1.8 m (w/h = 1.6) does not retain a solid core.

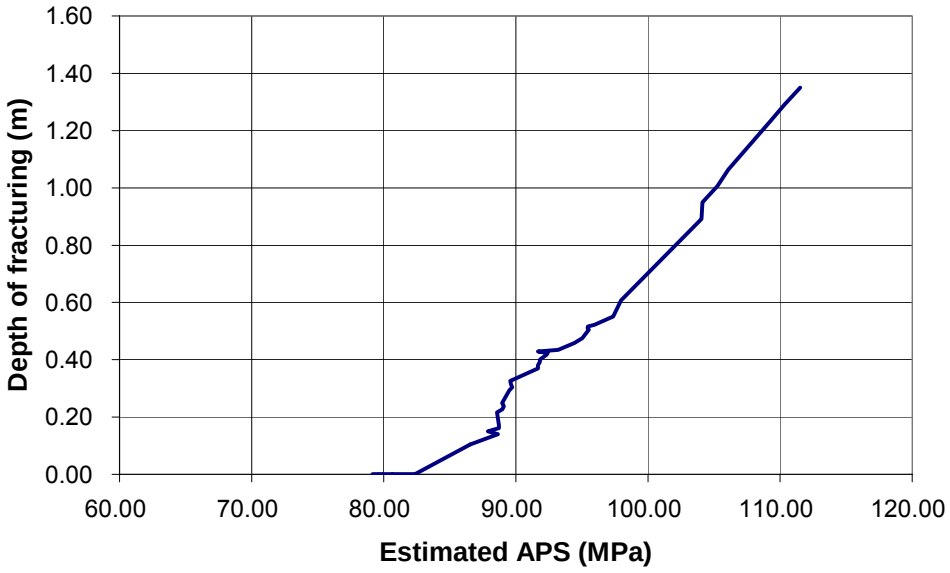

Figure E 52 Depth of fracturing into the pillar sidewall, inferred from the P1a measurements

The correlation between the measured and elastic horizontal stresses is shown in Figure E 53. The results in the figure represent the horizontal stresses about 67° to the pillar sidewall. The measurements were tracked by the elastic model reasonably well up to 4 April 2007, but significant differences occurred after this and the horizontal stress in the hangingwall above the pillar continued to increase

even after pillar failure. The higher than elastic stresses suggest some form of pillar punching, which may have caused the additional fracturing observed in the second borehole camera survey, which was performed after the panels had been mined. About three months after pillar failure, the horizontal stress above the pillar appears to have dropped to similar levels to the vertical stress (Figure E 54).

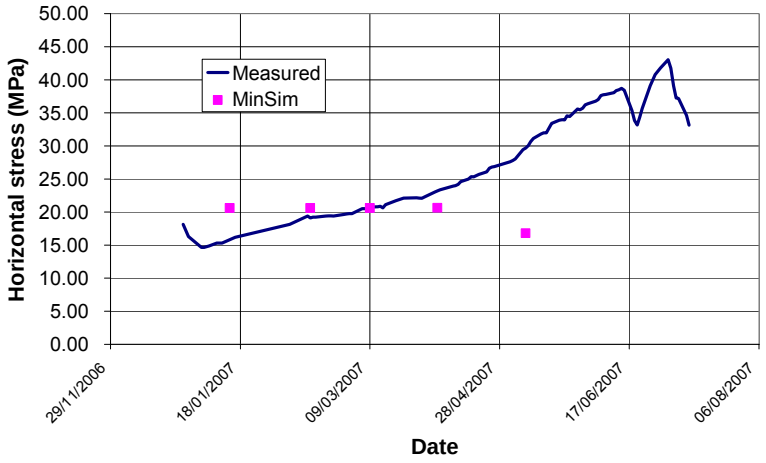

Figure E 53 Horizontal stress 5.3 m above the instrumented pillar

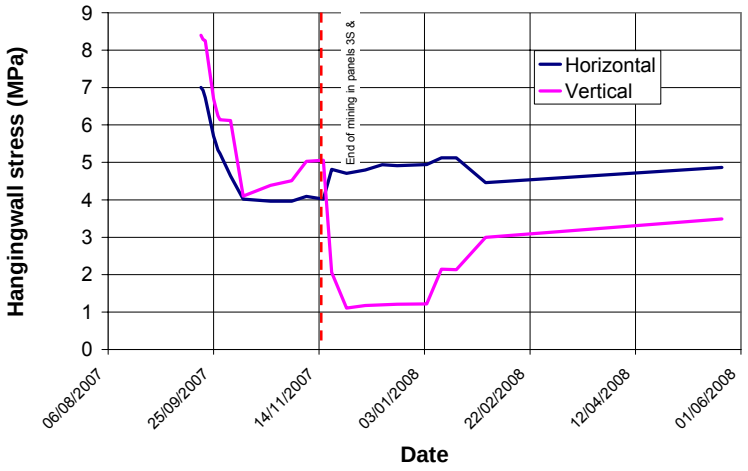

Figure E 54 Horizontal and vertical stress change 6.86 m above the instrumented pillar. The horizontal measurement is perpendicular to the pillar edge

Horizontal stress measurements were made in a vertical borehole drilled into the hangingwall at the centre of a stope after mining had been completed in the area as shown in Figure E 46. The immediate hangingwall conditions at the site were poor with shallow and steeply dipping joints. Due to the hangingwall conditions large areas were unmined and the stope span was much smaller than at the other instrumentation sites. The results of the investigation are plotted as a function of height above the stope and compared to elastic models with k-ratios of 0.5 and 2.0 in Figure E 55. The observed open discontinuities (borehole camera survey) and the lithology have also been included in the graph. The first four measurements (0 m – 10 m) show the type of profile expected for beams, although the magnitude of the fourth measurement is unrealistically high. In addition the following three measurements are unbelievably high, indicating a very high k-ratio in the lighter leuconorites and anorthosites. As borehole breakout was not observed in the borehole camera survey, the quoted stresses are probably too high but the profile is likely to be correct and the stresses are believed to be significantly higher in these rocks than the darker rock-types at this site. The Bastard Reef pyroxenites appear to have a k-ratio of about 0.5.

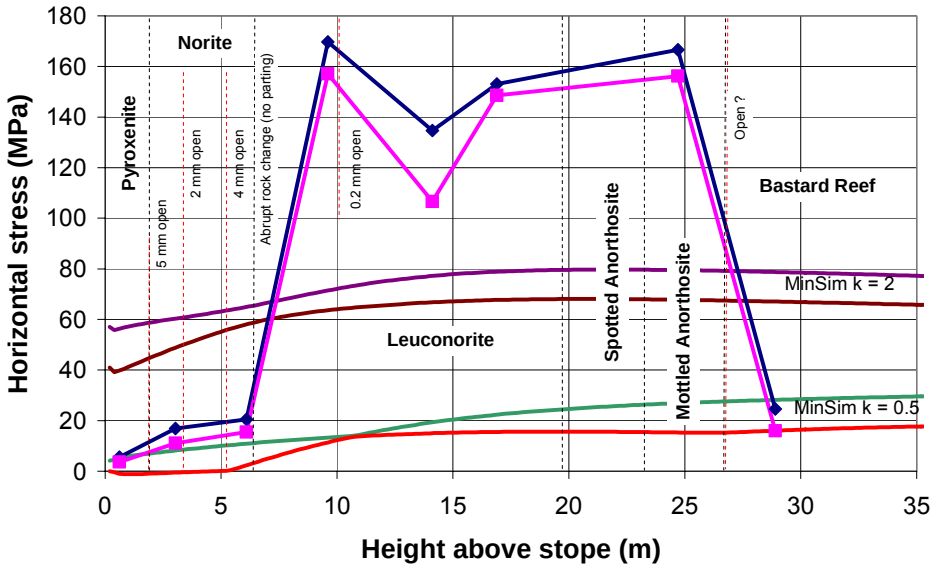

Figure E 55 Horizontal stresses above the stope shown in Figure E 46

E3 Footwall investigations

E3.1 Impala 10-shaft

E3.1.1 Location

The 17 south drive was developed about 16 m below the planned 7s and 8s panels. A vertical borehole was drilled from the drive through the planned position of Pillar 2 (CSIRO2 in Figure E 56), ahead of both panels. Borehole F/W1 (Figure E 56) was drilled at a late stage of the stope evolution, when Panel 7s was far advanced and Panel 8s was 15 m from its final position. The borehole was intended for the installation of an extensometer and drilled downwards from the stope to a depth of 12.6 m. It was located approximately 6.5 m to the east of the haulage hole and 4.9 m down-dip of Pillar 2. The stope entrance was through a travelling way developed into Panel 8s (Figure E 56), which was over-stoped some years before the investigation.

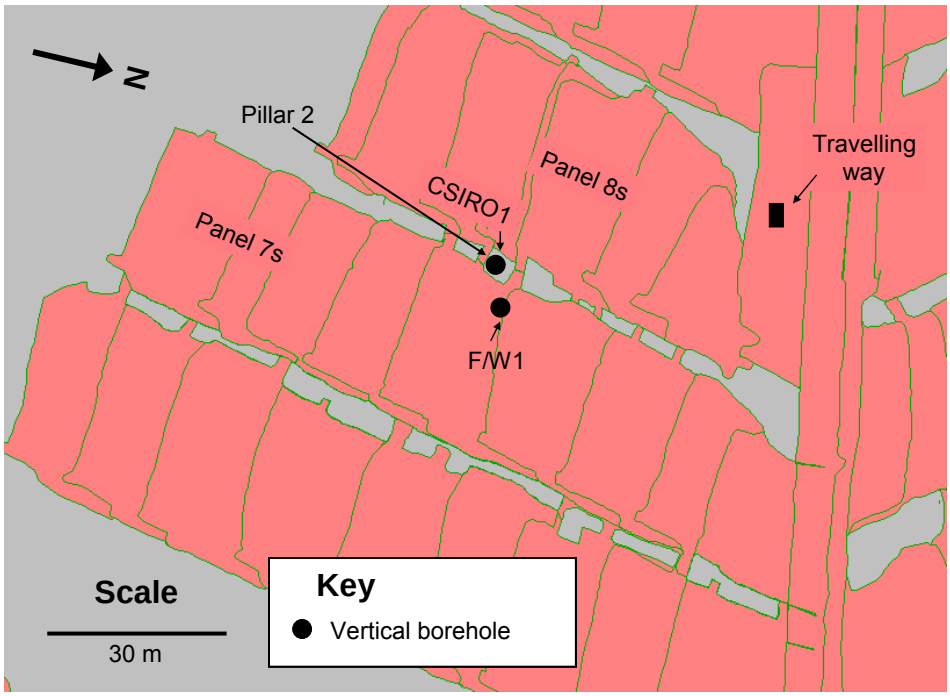

Figure E 56 Stope sheet showing the the vertical boreholes drilled through the footwall and the location of the travelling way entrance

E3.1.2 Observations

Only one steeply dipping discontinuity was observed in the footwall core of Borehole CSIRO1, at about 1.3 m below the stope. High horizontal stresses were evident from core discing in the immediate footwall (spotted anorthosite) and mottled anorthosite in the stope area (Figure E 57). A k-ratio of about 1.4 was estimated from sockets in the drive. Approximately 30 m to the south, where the 17 and 17A south drives converged, significant gothic arching was observed (Figure E 58), suggesting a k-ratio of at least 1.4 on this elevation.

Figure E 57 Core disking observed in the F/W anorthosites

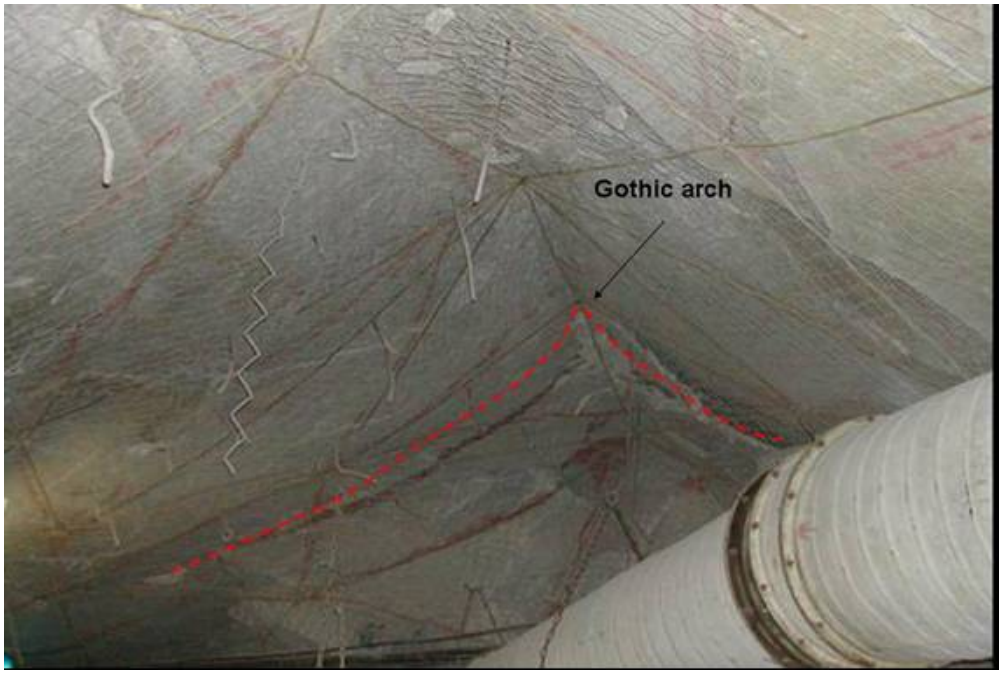

Figure E 58 Gothic arching in the 17 South Drive

The entrance to the stope was through a travelling way developed from the drive into the 8s panel (Figure E 28), Near the top of the travelling way, approximately 1.3 m below the stope footwall a parting plane had opened about 30 mm (Figure E 59). The feature was obviously a fault plane with striation planes and calcite/serpentinite filling (Figure E 60). During mining operations, the immediate footwall appears to have sheared on the discontinuity, displacing on strike about 60 mm away from the face (with respect to the rock below the discontinuity - Figure E 60). This discontinuity was not observed in the 17south drive borehole.

Figure E 59 Open discontinuity observed in the travelling way 1.3 m below Panel 8s

Figure E 60 Striations on the discontinuity surface, indicating a fault

E3.1.3 Borehole camera survey

The survey was conducted in F/W1 (Figure E 56) at the time of drilling the borehole. Small pieces of core were drilled in the first 8 m (Figure E 61) probably

due to a worn core-spring but may have been discing, indicating high horizontal stress. Water losses were recorded during drilling, showing that there were open discontinuities prior to drilling the hole. A sudden change in lithology was observed at 1.37 m below the stope. No geological discontinuities were visible in the first 9 m and only one steeply dipping joint between 9 m and 10 m.

Figure E 61 Core from F/W1 (Figure E 56)

The water accumulated in the borehole was ejected using compressed air, but once the pipes were removed water ingress from fractures could be clearly seen. A borehole camera survey was conducted to a depth of 7.95 m, where the level of the water at the time blocked the vision. The observations are summarised in Table E 4. Most of the open fractures were observed within 3 m of the stope.

Table E 4 Borehole camera survey in the F/W extensometer hole

Depth below the stope (m)	Aperture (mm)	Dip angle (degrees)	Comments
0.60	0.2	10	
0.63	0.5	10	
1.58	0.8	10	
1.59	0.5	10	
1.98	0.5	48	
2.18	0.8	10	Water ingress
2.53	1.0	45	Water ingress
4.20	0	10	Not clear
7.95			Top of water

Significantly more discontinuities/fractures were observed in the borehole drilled behind the face (F/W1) than ahead of the face (CSIRO1). Unfortunately no stress measurements were conducted in the footwall.

E3.1.4 Extensometer results

The results of the footwall extensometer in CSIRO1 (Figure E 56) are compared to an elastic model in Figure E 62. Two elastic models were run. The first assumed the matrix elastic constants for the hangingwall anorthosites (E = 83 GPa and v = 0.32) and the second assumed the constants derived for the footwall anorthosite (E = 110 and v = 0.28). The first model showed identical final deformations, but the model results prior to the pillar failure provided positive deformations that were greater than the measured. (Positive deformations refer to compression.) The good correlation between the elastic and the measurements before pillar failure in the second model suggests that the rock mass was behaving in an elastic manner with the same modulus as an intact rock sample. The under-estimation of the deformations after pillar failure could be because the wrong residual strength was used for the failed pillar (30 MPa), that some inelastic pillar punching deformations occurred or a combination of both. In all cases the possible inelastic, punching deformations are small.

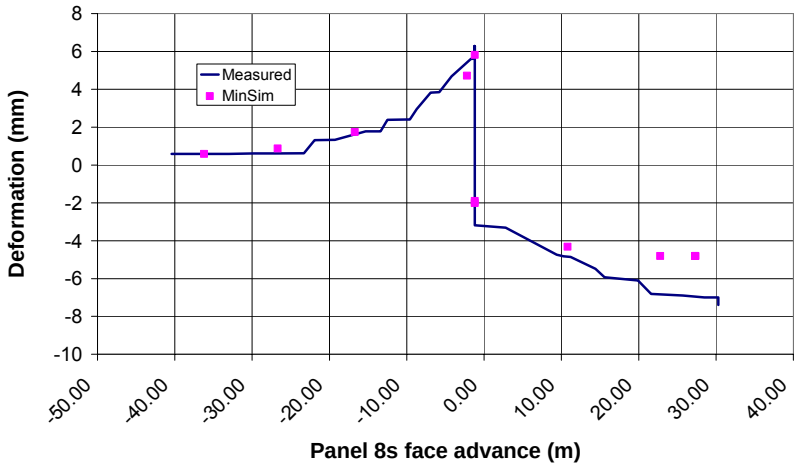

Figure E 62 Footwall extensometer below the centre of Pillar 2, plotted against the advance of the 8s face. Negative face advances represent the face position behind the instrument

The deformations measured in the extensometer in Borehole F/W1 (Figure E 56) were less that the accuracy of the instrument and indicate that little or no inelastic deformations occurred in the 7S panel footwall, to a depth of 12.57 m, since the instrument was installed.

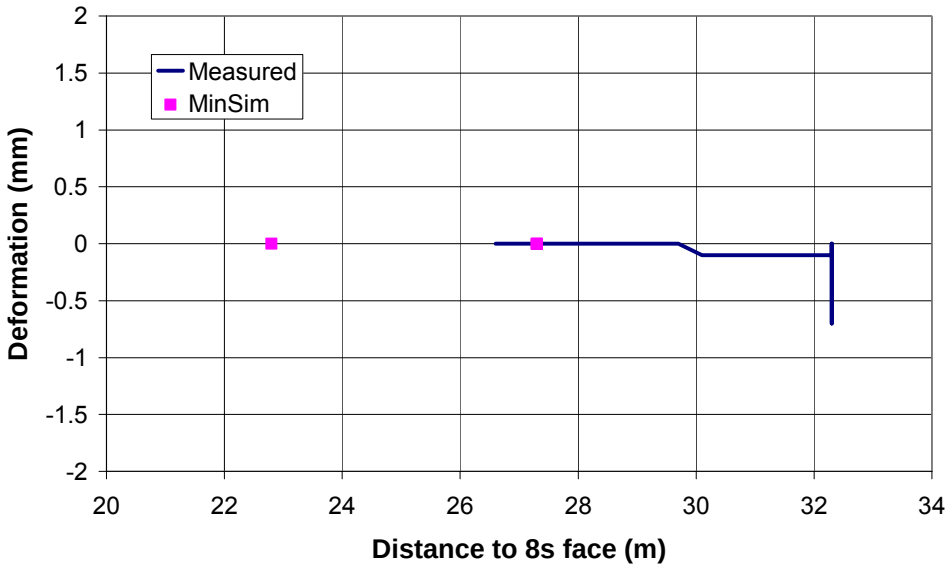

Figure E 63 Results of the footwall extensometer installed in F/W1 (Figure E 56), to a depth of 12.57 m below the stope

E3.2 Union Spud shaft

E3.2.1 Location

An extensometer was installed about 6.3 m from the edge of the instrumented pillar from the bottom of the centre gully, about 1 m below the stope. The location of the extensometer borehole is shown in Figure E 64.

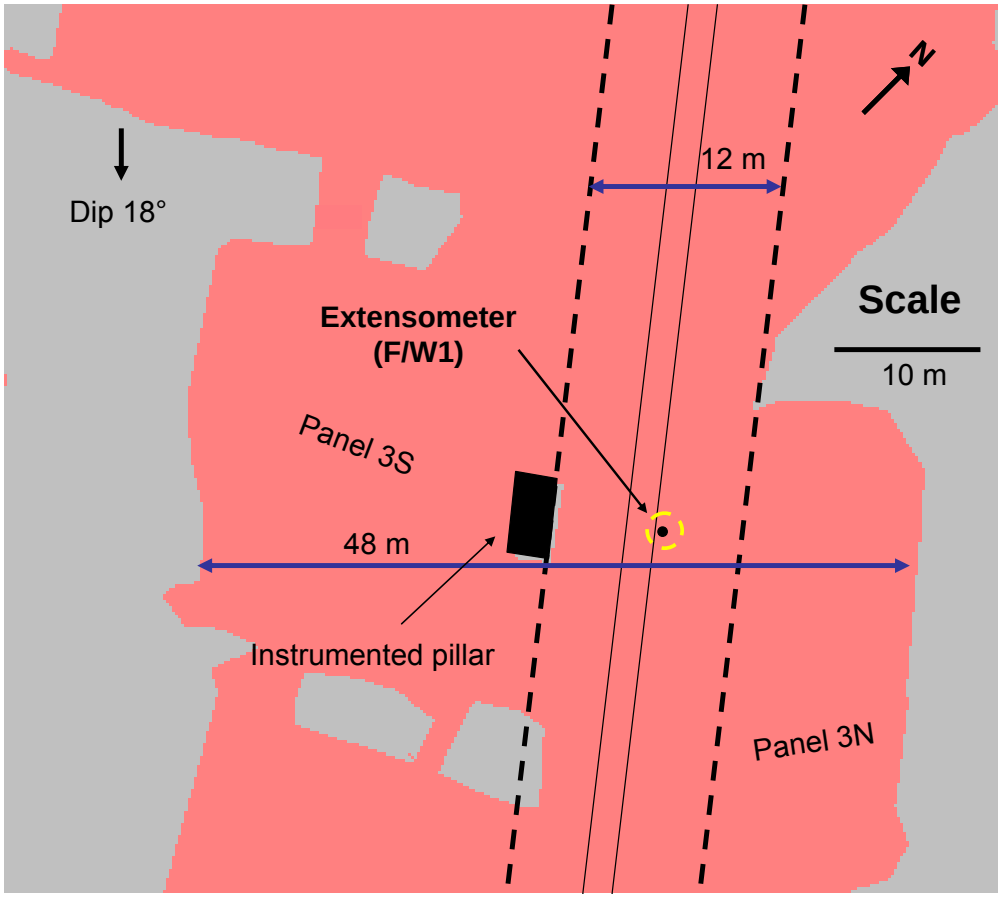

Figure E 64 Stope sheet showing the location of the footwall extensometer at Union Spud shaft

E3.2.2 Observations

Borehole F/W1 (Figure E 64) was drilled when the stope was in ledging stage, with a strike span of 12 m. The core that was retrieved from the borehole is shown in Figure E 65. Each row represents 1 m and the borehole started approximately 1 m below the stope, i.e. from the bottom of the centre gully. The footwall was significantly more fractured than the hangingwall and consequently more difficult to drill, particularly near the stope. The closely spaced fracturing up to about 3 m (4 m below the stope) indicated the depth of fracturing, which extended to the base of the Pseudo Merensky lithology. The closely spaced fracturing between 1.62 m and 2.17 m (2.62 m and 3.17 m below the reef)

appeared to be disced suggesting high horizontal stresses in the Pseudo Merensky. The immediate footwall is known colloquially as “Tarentaal” and appears to be heavily jointed with mainly steeply dipping joints. The unusual rock type in the immediate footwall shows that the reef is being mined from the bottom of a large pothole. The darker rock between 11.16 m and 12.32 m is the UG2 Reef, chromitite package. There was no anorthosite in the 19.5 m long borehole that was drilled into the footwall (20.5 m below the stope) and the predominant rock type is pyroxenite. Most of the joints in the footwall rocks appear to be steeply dipping, but the rock is stratified in the UG2 package creating possible planes of weakness along which slip could occur. However, signs of slip were not obvious on these planes at the time of drilling the borehole.

Figure E 65 Borehole core retrieved from Union Spud shaft F/W1

E3.2.3 Borehole camera survey

Only the first 4 m were visible as water was running into the borehole from the many open discontinuities. As the collar of the borehole was located at the bottom of the centre gully (Figure E 64), 1 m should be added to the depths of the discontinuities and fractures in Table E 5 to determine their depths below the stope. Water was observed to be running out of a discontinuity at 1.15 m or 2.15 m below the stope.

Table E 5 Discontinuities and fractures observed in a borehole camera survey conducted in the footwall in borehole F/W1 (Figure E 64)

Depth below the collar (m)	Aperture (mm)	Dip angle (degrees)	Comments
0.37	0.1	80	
0.37	0.3	20	
0.60	0.3	20	
1.00	0.3	20	
1.15	0.5	20	Water ingress
1.35	0.5	20	
2.60	0.5	20	
2.90	0.5	20	
3.50	1.0	90	
4.30	-	20	Lithology change
Water level prevented further observations			

E3.2.4 Extensometer results

The extensometer installed in borehole F/W1 was a single anchor instrument measuring deformations that occurred between the base of the centre gully (1 m below the stope) and 19 m below the stope. In an adjacent borehole an anchor was installed 5.5 m below the stope and was referenced against the hangingwall, thus measuring closure. These results were subtracted from a nearby closure meter to provide the deformation that occurred in the immediate 5.5 m of the

footwall. Unfortunately the model showed slightly different elastic convergences between the two closure meters when the 3N panel was mined and therefore only the initial deformations are shown in Figure E 66. The results of the extensometers are compared to an elastic model with elastic constants of E = 60 GPa and v = 0.32 in the figure. These constants were already significantly lower than the laboratory derived values but are included to show that significant inelastic deformations occurred in the footwall. A comparison between the two measurements and the elastic model suggests that all the inelastic deformation occurred in the upper 5.5 m before the instrumented pillar failed. However after pillar failure significant deeper-level deformations appear to have occurred, even though the pillar was 6.3 m from the extensometer.

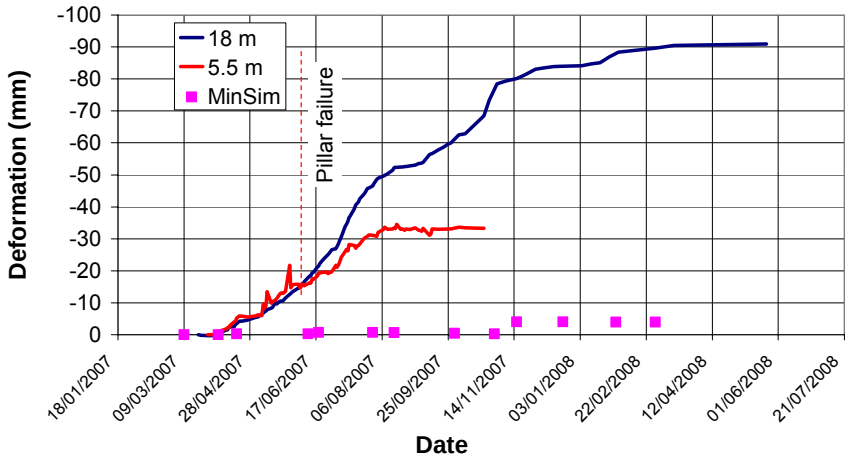

Figure E 66 Footwall extensometer results showing the deformations that took place down to depths of 5.5 m and 19.0 m below the stope. The anchor at 18 m measured to the bottom of the centre gully

Figure E 67 shows a comparison between the footwall and hangingwall extensometer results. Significantly more deformation was measured in the footwall than the hangingwall in spite of the shorter length of the footwall extensometer. The first sharp increase in the deformation rate coincided with the barring of 0.5 m from the edge of the pillar, along half the pillar on the down-dip side. This accelerated deformation also coincided with a drop in the pillar stress. More deformation was measured in the footwall than the hangingwall suggesting

that some footwall punching was occurring. The second sharp increase in closure rate occurred when the 3N panel started mining. The reason for the larger hangingwall deformations during this period is not clear.

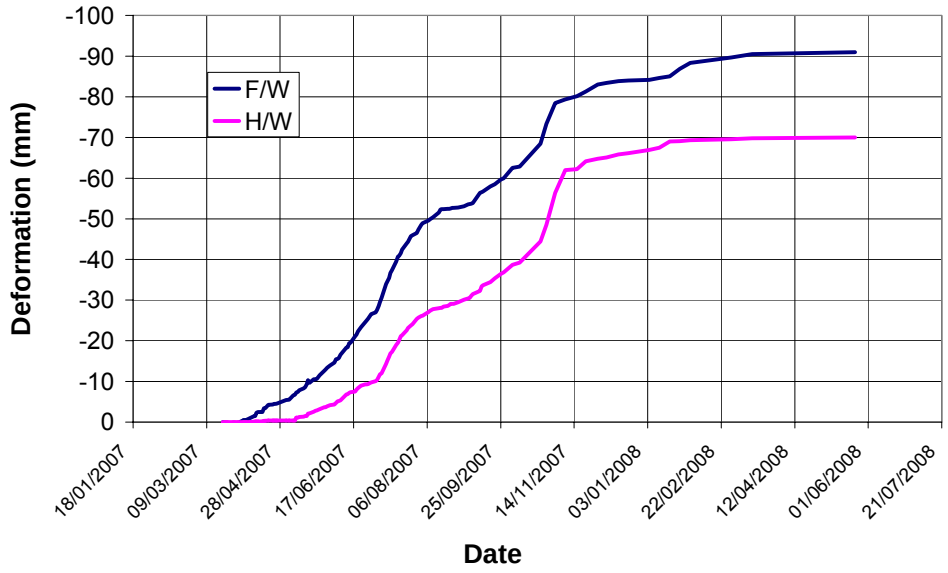

Figure E 67 Comparison between the footwall and hangingwall extensometer results

E4 References

Jenkinson, D. (2006). Pers. Comm., Impala Platinum Mine, RSA.

Napier, J.A.L. and Hildyard, M.W. (1992). Simulation of fracture growth around openings in highly stressed, brittle rock, *J. S.A. Inst. Min. and Metall.,* Vol. 92, no.6, pp. 159-168.

Watson, B.P. (1996). Instrumentation of a stope at Union Section, Richard Shaft, *Confidential report to the mine.* COMRO, Johannesburg, RSA.

York, G., Canbulat, I., Kabeya, K.K., Le Bron, K., Watson, B.P. and Williams, S.B. (1998). Develop guidelines for the design of pillar systems for shallow and intermediate depth, tabular, hard rock mines and provide a methodology for assessing hangingwall stability and support requirements for the panels between pillars, *SIMRAC project GAP 334*, The Safety in Mines Research Advisory Committee (SIMRAC), Braamfontein, RSA.